Journal of Atmospheric and Solar–Terrestrial Physics 211 (2020) 105474

Contents lists available at ScienceDirect

Journal of Atmospheric and Solar-Terrestrial Physics

journal homepage: www.elsevier.com/locate/jastp

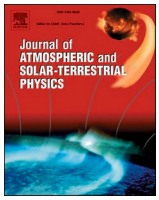

Research Paper

Substorm onset and development: The crucial role of flow channels

Larry R. Lyons [a,*], Yukitoshi Nishimura [b]

[a] Department of Atmospheric and Oceanic Sciences, University of California, Los Angeles, CA, 90095-1565, USA
[b] Center for Space Physics and Department of Electrical and Computer Engineering, Boston University, Boston, MA, 02215, USA

ARTICLE INFO

Keywords:
Substorm
Flows channels
Streamers
PBIs
Flow bursts

ABSTRACT

In this paper, we described the basic features and observations bases of the scenario for the substorm expansion phase that we have developed from our research over the past ~10 years. Onset occurs along magnetic field lines of the inner proton plasma sheet, and is first seen in the aurora as beading along the onset aurora arc, which lies near the equatorward boundary of the auroral oval. Growth of these onset waves and large amplitude electric field oscillations indicates that an abrupt transition from a stable to unstable state leads to onset. The transition to instability occurs as a result of an intrusion of a low-entropy flow burst/channel (i.e., a plasma bubble) to the inner plasma sheet, and such flow bursts are marked in the auroral oval by the initiation of a poleward boundary intensification (PBI) that evolves into an auroral streamer. Plasma flows associated with these and other PBIs are generally associated with enhanced reconnection at the distant tail neutral line, the reconnection being triggered by an incoming flow channel from the polar cap. It is reasonable that the onset instability is triggered by the intruding reduced entropy plasma abruptly changing the entropy distribution in the inner plasma sheet, though the specific onset instability has not been identified. The onset instability is azimuthally aligned and expands azimuthally, these occurring because, as a bubble moves earthward, lower energy ions tending to follow the electric field drift towards the dawn side while higher energy ions magnetic drift towards the duskside. Thus entropy is not conserved along center of mass drift trajectories, and the bubble spreads in longitude and deepens. The transition to non-linearity of the growing onset waves leads to streamers. How this occurs is another major outstanding question, but the first streamers could initiate within the plasma sheet ~20 R_E downtail, the region where reconnection has been inferred to occur soon after onset. It is likely that streamers and their associated reconnection initiate at the distant tail neutral line once the expansion phase auroral activity reaches the auroral poleward boundary. The substorm current wedge builds up from a sequence of longitudinally localized flow burst regions (wedgelets) that are associated with the expansion-phase streamers, dipolarize the local magnetic field, and give rise to traditional ground onset signatures on the ground, namely auroral zone H bays and mid-latitude positive H bays and Pi2 pulsations.

1. Introduction

Substorms are a disturbance of the global magnetosphere-ionosphere system. They have varying sizes and durations, and large ones release large amounts of solar wind energy accumulated in the magnetotail (e.g., Rostoker et al., 1980). Substorm expansion phase onset is characterized in the aurora by an initial brightening that occurs along a pre-existing, growth-phase arc that emerges near the equatorward boundary of the auroral oval (Akasofu, 1964; Samson et al., 1992; Deehr and Lummerzheim, 2001). The growth phase arc is latitudinally narrow, is oriented approximately in the east-west direction, and stays dim for a few to tens of minutes near the end of the substorm growth phase (Nishimura et al., 2011a, and references therein). The initial brightening occurs along a section of the growth phase arc, and the brightening then expands in longitude along the growth phase arc (Lyons et al., 2013b; Sakaguchi et al., 2009; Shiokawa et al., 2009). The brightening appears as beads along the growth phase arc (e.g., Donovan et al., 2006; Liang et al., 2008, 2018; Rae et al., 2010), such beading being seen for virtually all onsets having good auroral viewing (Kalmoni et al., 2017; Nishimura et al., 2016). The auroral beads propagate azimuthally and evolve into wavy structures, indicating that the beads are an auroral manifestation of waves associated with an onset instability.

The onset brightening occurs near the inner edge of the electron auroral oval and where precipitating protons have been energized to

* Corresponding author.
E-mail addresses: larry@atmos.ucla.edu (L.R. Lyons), toshi16@bu.edu (Y. Nishimura).

https://doi.org/10.1016/j.jastp.2020.105474
Received 29 June 2020; Received in revised form 12 October 2020; Accepted 15 October 2020
Available online 31 October 2020

energies of the growth-phase, partial ring current (which equates to the inner region of the proton plasma sheet) (Samson et al., 1992). The onset is not at the peak of proton precipitation, which would map to the center of the partial ring current, but within the poleward gradient of the proton precipitation (Deehr and Lummerzheim, 2001; Liang et al., 2018) that maps to the equatorial region where the magnetic field transitions from being highly stretched to more dipolar (e.g., Donovan et al., 2008; Sergeev et al., 2012, and references therein). Consistent with this mapping, the onset arc within or at the poleward edge of the Region 2 field-aligned current (FAC) region at the onset longitude (Nishimura et al., 2012a, 2012b).

Two examples with good auroral viewing of what is seen at and following the initiation of substorm auroral onset are shown in Fig. 1, which displays a sequence of combined auroral images from the THEMIS all-sky imager (ASI) array over North America (Mende et al., 2008) for each event. The onset beads initially appear as faint rays (seen by the convergence of auroral brightenings toward the center of each imager's field-of-view (FOV)) identified by yellow arrows in Fig. 1Aa and Ba. The beads are initially seen to extend in very nearly the east-west direction over a limited longitudinal range. The beads are regularly spaced like waves, and they then grow in intensity (Kalmoni et al., 2017; Nishimura et al., 2016) as the region of detectable wave structure spreads in longitude, the spreading indicated by orange arrows in Fig. 1Ac-e and Figures Bb and Bd. The beads show wave-like structure that grows in amplitude exponentially (Kalmoni et al., 2017), and soon develop non-linearities that form the active aurora of the substorm expansion phase (identified by yellow arrows in Fig. 1Ad-g and Bd-h. These growing waves are the classic signature of an instability that grows and until it becomes non-linear. Two east-west keograms of differential intensity along the onset arc shown in the lower panels of Fig. 2 to give a different view of the growth and longitudinal expansion of the waves, and their evolution into the bright substorm expansion phase aurora. The event in Fig. 2A is the same as the event in Fig. 1B. Initial onset of visible waves covers roughly 5° in longitude. Growth and longitudinal spreading of the region of waves can clearly be seen, along with the eastward (for these events) phase velocity of the waves. The middle panel is the maximum emission intensity along the onset arc, and this can be seen to gradually increase until more explosively increasing when the non-linear development leads to poleward expansion of the region of active aurora.

The beads can be seen simultaneously in both hemispheres with similar wavelengths and periodicities (Motoba et al., 2012), indicating that the beads are generated by plasma sheet plasma rather than in the auroral acceleration region or in the ionosphere. Otherwise, different ionospheric conditions would create different characteristics of waves in the different hemispheres. Additionally, highly fluctuating magnetic fields in the near-Earth plasma sheet have been suggested to be linked to a magnetospheric substorm onset instability (Takahashi et al., 1987; Lui, 1996; Ohtani, 1998; Shiokawa et al., 2005). The longer period component of those fluctuations (several tens of seconds) corresponds to periods seen in the aurora as the beads pass overhead. Consistent with this, Rae et al. (2010) reported that, at auroral onset, frequencies are ~30–90 s in the aurora and in the ground magnetic field, and waves with similar frequencies have been seen within the inner plasma sheet preceding substorm-related magnetic field dipolarizations and having characteristics expected from plasma sheet instabilities (Cheng and Lui, 1998; Park et al., 2010; Roux et al., 1991). While no study has yet evaluated the connection of the oscillations in the tail to optical onset waves/beads, such a connection appears likely and both are likely be signatures of what can be referred to as the "substorm onset instability". It is important to note that the instability does not appear to create a new wave mode along onset arc field lines, but instead causes the transition to instability of stable waves that exist along those field lines prior to onset (Nishimura et al., 2014; Panov et al., 2012; Uritsky et al., 2009).

A quite dramatic feature of the instability is its electric field signatures as seen by ground radars (Gallardo-Lacourt et al., 2014b). Fast oscillating flows (~1000 m/s) are correlated with the onset beads as they propagate across the meridian of a poleward looking radar beam, and 2-d radar measurements show a wavy pattern in the azimuthal direction with a wavelength of ~80 km, which is approximately the same of azimuthal separation of individual beads. The association between the flow oscillations and beads can be seen in a time-series format in Fig. 3. The two panels in Fig. 3a show an auroral east-west auroral keogram along the magnetic latitude of the beading and the latitudinal profile of the flow velocity measured by the high-time resolution meridional-looking beam 6 of the SAS SuperDARN radar. This figure clearly illustrates that strong oscillating flows initiate with the onset (identified with a red line) and continue for a few minutes. A zoom in around the time where the beads are observed in shown Fig. 3b. From top to bottom, the panels show a north-south auroral keogram along the SAS radar beam 6, a zoomed in version of the east-west keogram in Fig. 3a, and the average flow velocity along the SAS radar beam 6. The vertical gray dashed lines give the times when each bead crosses the radar beam longitude (white horizontal line in the east-west keogram), and each auroral bead is marked by a white dashed line in the east-west keogram. The orange and blue arrows in the third panel represent equatorward and poleward flow enhancements, respectively. As auroral bead crosses the radar beam longitude, we see an equatorward flow

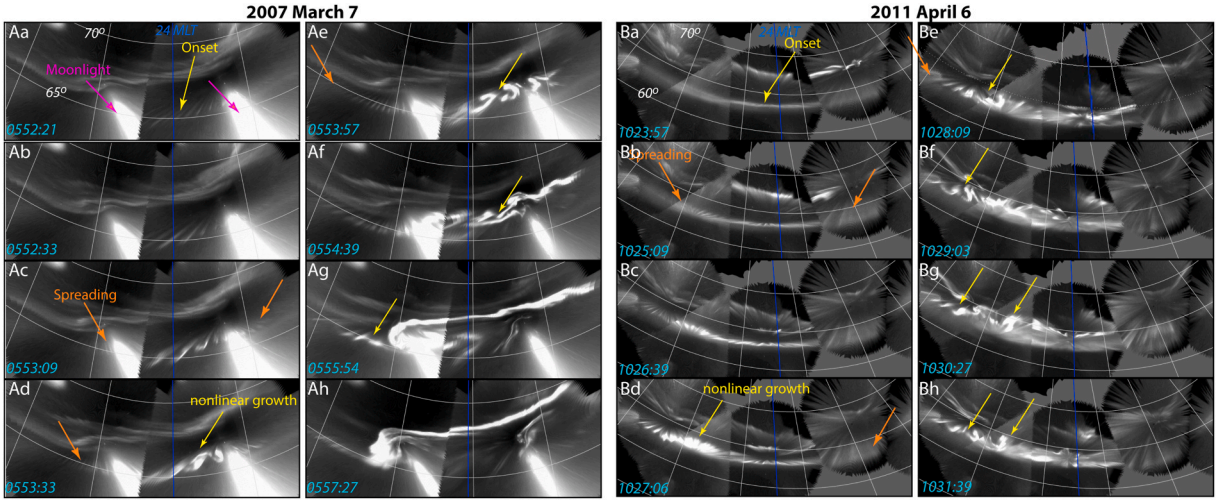

Fig. 1. Selected mergers of the auroral images from the THEMIS ASIs for the time interval of substorms on (A) 2007 March 7 and (B) 2011 April 6. The dark blue line marks magnetic midnight, and longitude lines are space 1 h in MLT apart. Moonlight contamination is identified in the first panel of (A).

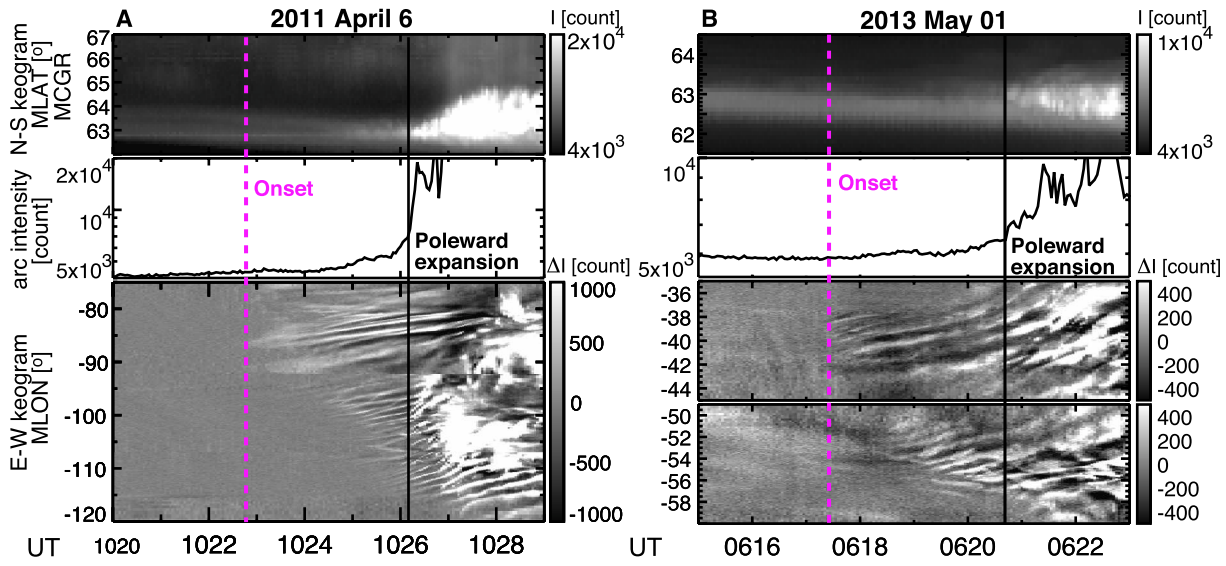

Fig. 2. From top to bottom, north-south auroral keograms, maximum intensity along the onset arc, and east-west auroral keograms in 5-min detrended intensity scales around onset times for substroms on (A) 2011 April 6 and (B) 2013 May 1. The dashed magneta and black vertical lines mark, respectively, the initial auroral brightening and the initiation of poleward expansion. North-south keograms use maximum intensity within ±15° longitude from imager zenith longitude at each latitude. East-west keograms are sliced along the initial brightening arcs (based on Nishimura et al., 2016).

enhancement followed by a poleward flow enhancement. Since the onset arc is oriented essentially perpendicular to the north-south radar beam orientation, the measured flows can be interpreted as flows across the arc rather than a projection of flows tangential to the arc.

For understanding substorms, the first necessity is to understand what causes the substorm onset instability. It is also necessary determine what causes the transition from a stable system to an unstable system, and what is the resulting instability. Fundamental for this understanding is that the instability is along a nearly east-west oriented auroral arc the maps to the inner plasma sheet, and that the instability spreads longitudinally along this arc. It is also necessary to understand what causes the traditional substorm signatures, namely the magnetic field decrease on the ground, particle injections, formation of the substorm current wedge, and features of expansion phase aurora such as the westward traveling surge, auroral streamers, and the duration of expansion phase aurora. Here we review what our research has shown about these fundamental questions and their relationship to flow channels in the plasma sheet. For a more general review of substorms, refer to Nishimura, Y., L. R. Lyons (2019), Substorms and Storms, AGU Books on Solar/Heliosphere 2: The active magnetosphere, in press.

1.1. *Reduced entropy flow channels: the cause of transition to instability*

Auroral observations have given us important information about what leads to substorm onset and which must be accounted for. First off, as discussed above, substorm onset is clearly an approximately east-west-aligned, large-scale instability of the inner plasma sheet and its electromagnetically connected auroral ionosphere. Furthermore, the transition to instability is fairly abrupt, in that it occurs much faster than the several to 10's of minutes time scales for plasma sheet changes associated with large-scale convection. Thus something must occur that causes an abrupt change in conditions in the inner plasma sheet. Reconnection could cause an abrupt change in plasma parameters, but substorm onset in the plasma sheet is well earthward of the typical tail reconnection regions (beyond $x = -20R_E$).

Nishimura et al. (2010a, 2010b) reported a repeatable sequence of events leading to substorm onset in observations from the THEMIS ASI array that should be associated with an abrupt change in conditions in the inner plasma sheet. As shown by the example in Fig. 4, the pre-onset sequence starts with formation of a poleward boundary intensification (PBI) along the auroral poleward boundary, which lies nearly along the separatrix between open and closed magnetic field lines. A roughly north-south oriented (NS) auroral form (referred to as an auroral streamer) then extends equatorward from the PBI towards the equatorward boundary of the aurora oval, which may turn into enhanced auroral brightness that drifts azimuthally (westward or eastward for auroral onsets in the dusk-cell or dawn-cell, respectively). Onset occurs when the enhanced auroral luminosity region reaches to near the onset location, or substorm onset can occur near the location where the streamer first reaches to near a growth phase arc located near the equatorward boundary of the auroral oval. An optical connection between the streamer and the growth phase arc is not expected since, as discussed below, a streamer demarcates an adjacent flow channel. It is the plasma within the flow channel that is expected to directly connect to the onset location along the growth phase arc. This could be the flow adjacent to the streamer that approaches the growth phase arc or the flow adjacent to, and equatorward of, the azimuthally moving brightness that follows the flow from the streamer.

Using the known relation between auroral enhancements and plasma sheet flow as mapped to the ionosphere (de la Beaujardière et al., 1994; Gallardo-Lacourt et al., 2014a; Haerendel, 2011; Henderson et al., 1998; Lyons et al., 1999; Nakamura et al., 2001; Pitkänen et al., 2011; Sergeev et al., 1999, 2000; Zesta et al., 2000), the observed auroral sequence implies that new plasma crosses the polar cap boundary onto closed auroral oval/plasma sheet field lines (corresponding to localized reconnection in the distant tail) and then intrudes as a longitudinally localized flow channel to the equatorward/near-Earth region of the auroral oval/plasma sheet, leading to the onset instability. In the ionosphere, auroral streamers are expected to lie to the right of the direction of the associated enhanced flow channel, because the enhanced upward field-aligned currents within the auroral enhancement are fed by enhanced ionospheric Pedersen currents within the flow channel. When mapped to the plasma sheet, these flow channels are often referred to as "flow bursts" or "bursty bulk flows", which are generally believed to consist of depleted magnetic flux tubes (i.e., flux tubes with lower total entropy than the surroundings, sometimes referred to as "bubbles") (Dubyagin et al., 2010; Panov et al., 2010; Pontius and Wolf, 1990; Sergeev et al., 1996, 2012; Wolf et al., 2012; Xing et al., 2010; Yang et al., 2011). It is thus reasonable that the plasma sheet flow channels trigger the onset instability by bringing reduced entropy plasma to the

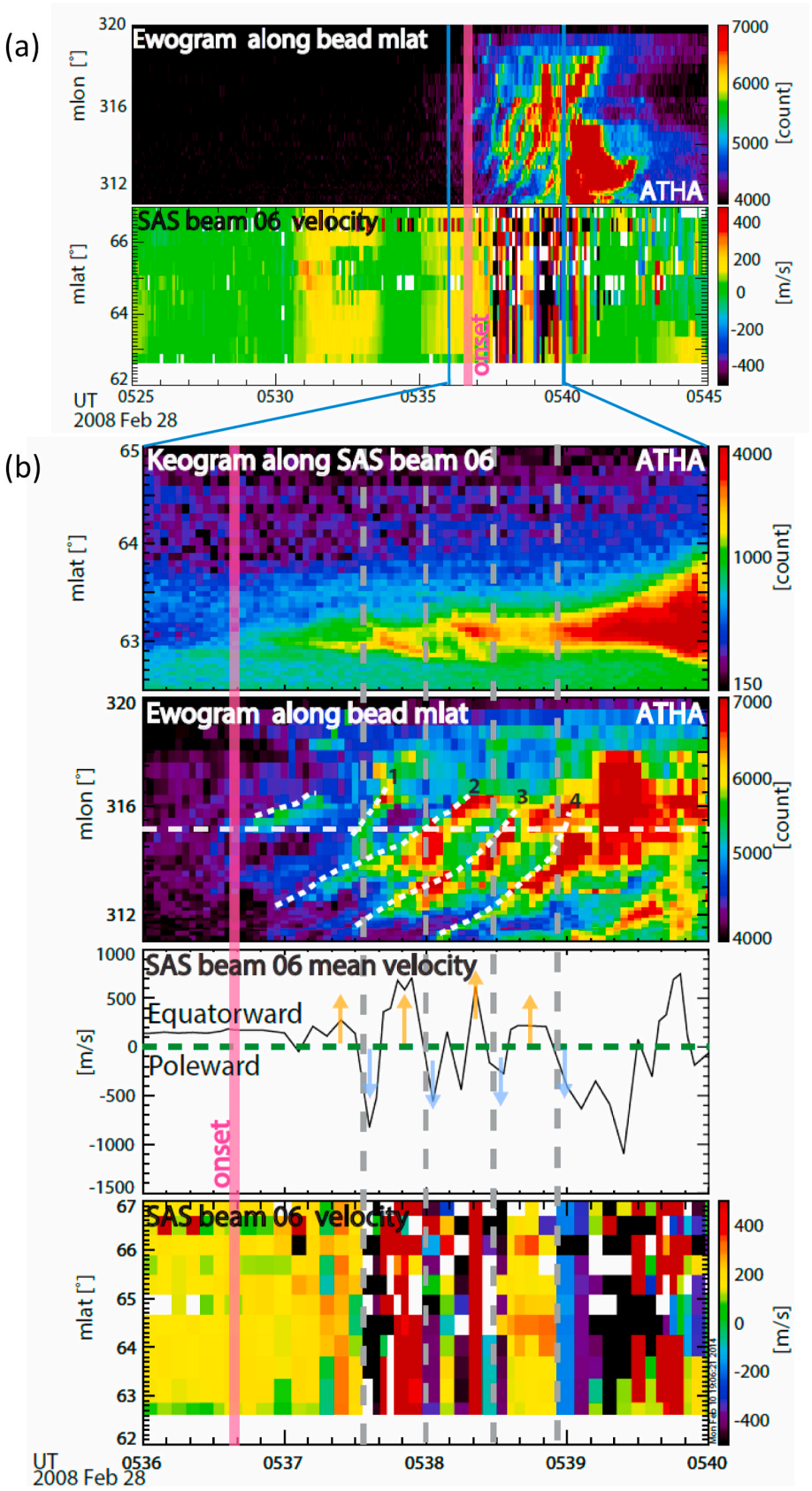

Fig. 3. (a) From top to bottom panels show an east-west keogram of the ATHA ASI along the bead magnetic latitude (~63 deg) and the ionospheric flow velocity measured by SAS beam 6 operating in the high resolution THEMIS mode along the magnetic meridian. (b) Blow up of the time inteval near substorm onset. From top to bottom, the panels show a north-south auoral keogram along the SAS radar beam 6, the east-west keogram along the beading magnetic latitude, and the average flow velocity measured by SAS beam 6. Pink vertical line indicates the onset time. The gray vertical dashed lines show the time when each bead crosses the radar beam longitude (horizontal white dashed line in the ewogram). Orange and blue arrows in the third panel show equatorward and poleward flow enhancements respectively (from Gallardo-Lacourt et al., 2014b).

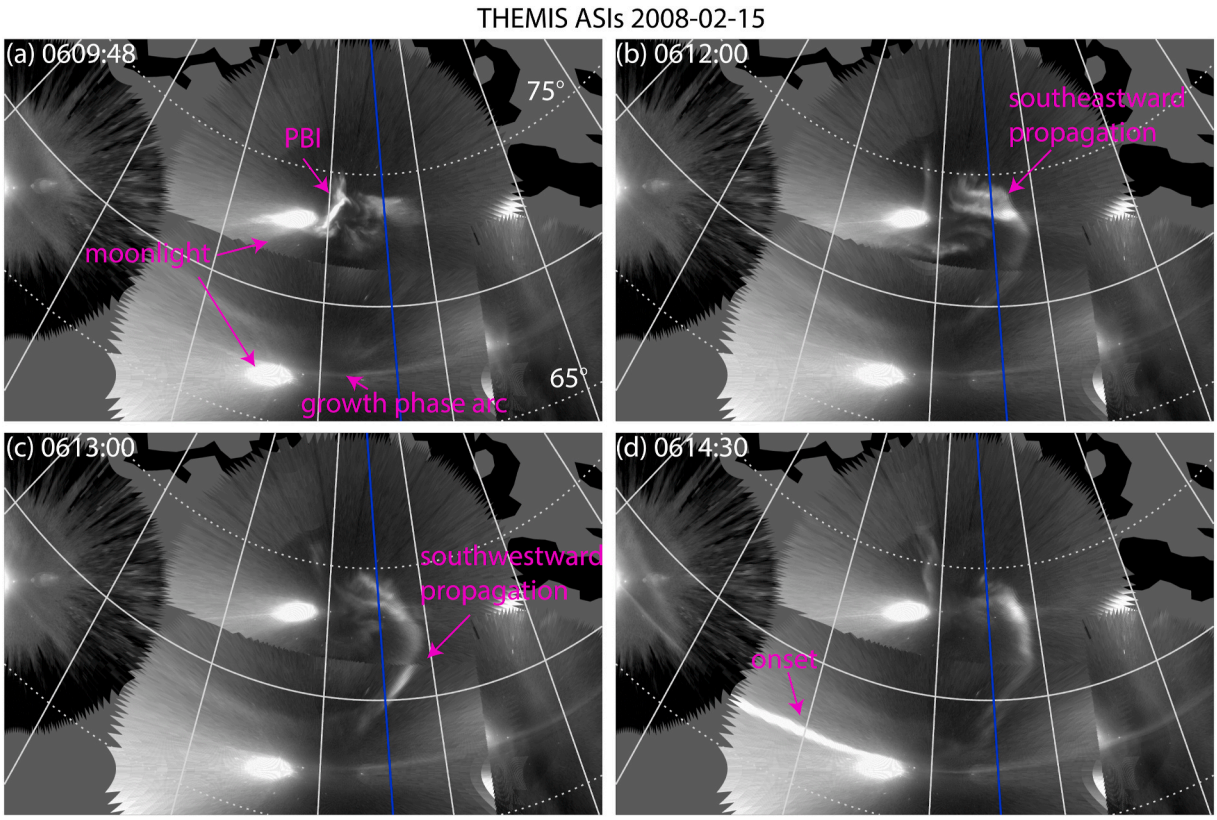

Fig. 4. THEMIS ASI data during an auroral onset on 15 February 2008. ASIs used are RANK, FSMI, and GILL. White lines are isocontours of magnetic latitude (every 10° in solid lines) and longitude (every 15°). The blue line in each panel is the magnetic midnight meridian. The onset occurred at 06:13:39 UT (based on Nishimura et al., 2011a, 2011b).

inner plasma sheet and abruptly changing the entropy distribution in the inner plasma sheet, the low-entropy plasma being brought earthward within a plasma sheet flow channel by interchange motion. In particular, it should lead to decrease in the tailward gradient of entropy, a gradient change that could be important (e.g., Xing and Wolf, 2007) for an abrupt transition to instability. This instability must be very different from just the earthward (equatorward as mapped to the ionosphere) interchange motion, since onset extends longitudinally along an east-west oriented auroral arc near the equatorward boundary of the auroral oval.

While there have been some debate about how often auroral streamers are seen leading to substorms (e.g., Frey, 2010), they are very commonly seen when viewing conditions are good and the auroral oval is not very thin making streamer identification from ASIs difficult (Lyons et al., 2018; Nishimura et al., 2010a, 2011a, 2011b). However, direct observation of flows in the ionosphere using radars allows a test of the flows to the onset location scenario without the ambiguities that can occasionally occur with auroral observations. An example from the initial study of such flows (Lyons et al., 2010a) is shown in Fig. 5. The top panes show the F-region velocity vector. (Flow vectors were from a Bayesian linear fit to line-of-sight (LOS) velocities using all PFISR beams under the assumption of no longitudinal variations with the radar FOV (Nicolls and Heinselman, 2007). See Lyons et al. (2010a) for LOS velocities.) Electron densities along two of the radar beams directed poleward along the magnetic meridian are shown in the second and third panels, respectively. Altitude is shown along the left axis and magnetic latitude Λ along the right axis. Ground magnetic observations are shown for two auroral stations approximately along the radar meridian and Pi2 observations from EAGLE at lower latitudes can be seen in the bottom panel. The time of the substorm onset identified by auroral imager observations is indicated by a dashed vertical line, and the latitude of initial substorm brightening (at $\Lambda \sim 66°$, (Zou et al., 2009)) is indicated by a star in the flow vector panel. The densities prior to the onset in Fig. 10 peak at ~130 km and fall off above ~150 km, which is a signature of the pure proton precipitation (Zou et al., 2009, and references therein) from the partial ring current that typically extends equatorward of the electron auroral oval and lies equatorward of the onset.

Starting at ~0710 UT, eastward flows can be seen in the poleward portion of the radar FOV and westward flows at lower latitudes, indicating the Harang reversal. Then, starting at ~0718 UT, a southeastward-directed flow enhancement moves equatorward and reaches the onset latitude at approximately the onset time. This corresponds to the cases of Nishimura et al. (2010a) in which onset occurs just when the equatorward-moving, NS-oriented auroral structure contacts the growth phase proton aurora. Onset occurs at the equatorward edge of the incoming southeastward-directed flow for this case. The substorm onset is seen in by a prompt enhancement in the E-region ionospheric densities seen by the radar and is followed by an ~500 nT magnetic bay and associated Pi2 pulsations at EAGL, a little equatorward of the onset latitude.

An example using nightside observations from the higher latitude Sondrestrom runs radar is shown in Fig. 6. The top shows panel flow velocities within the F-region as a function of Λ and UT. E-region electron densities at 130 km altitude, which respond to auroral electron precipitation, are shown in the second panel. The low-density values and noisier data seen prior to ~02 UT are indicative of the low energy flux of precipitations expected along open polar-cap field lines. The high values seen from ~0207 to 0220 UT are the expected result of the high fluxes of electron precipitation corresponding to intense aurora during the substorm expansion phase, and the intermediate values seen after that time indicate less intense electron precipitation from the plasma sheet. Auroral imaging was not available in the vicinity of Greenland for this event, but the Sondrestrom run were scheduled so that THEMIS spacecraft (Angelopoulos, 2008) were within the inner plasma sheet in

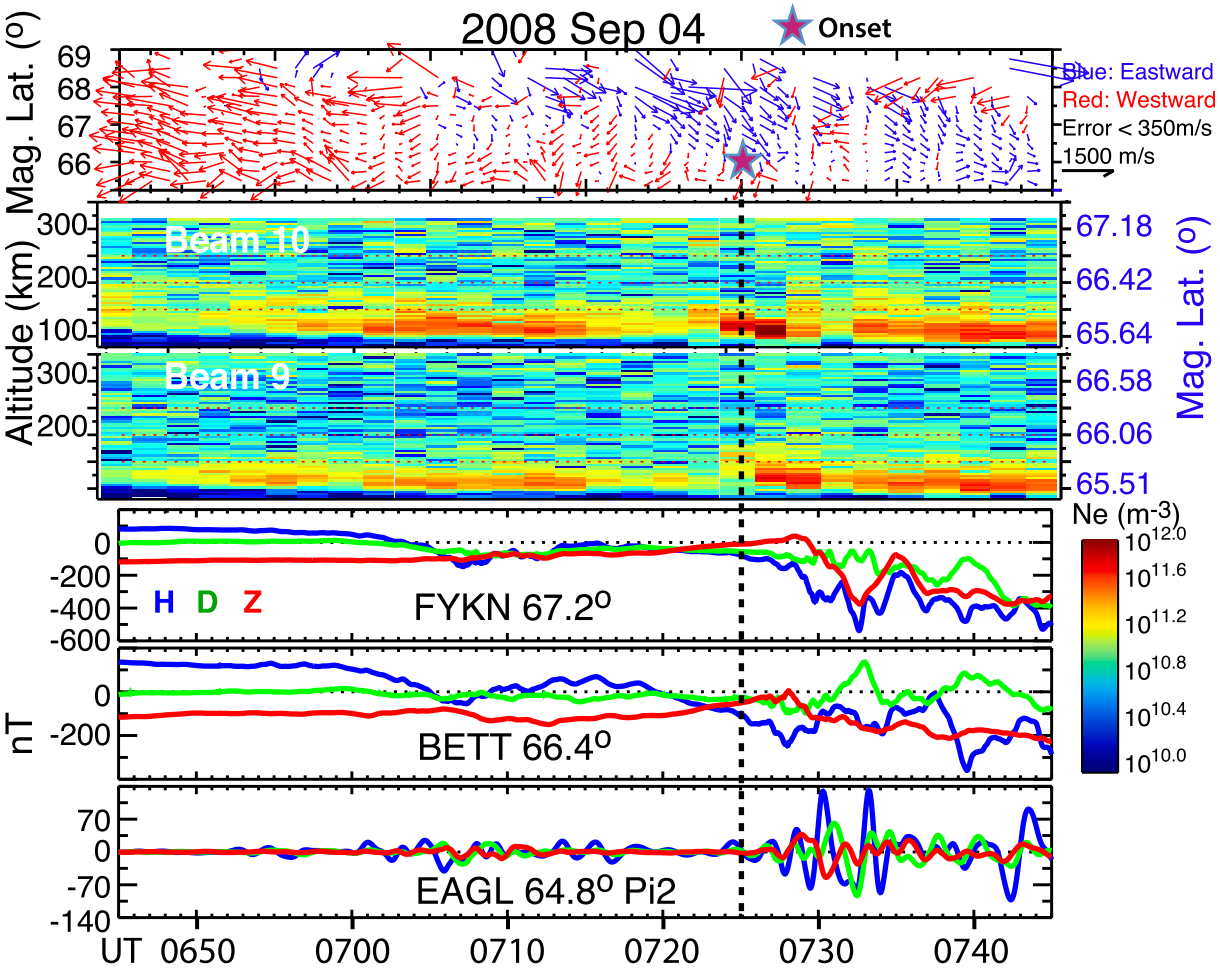

Fig. 5. PFISR observations from 0640 to 0750 UT on 4 September 2008. The top three panel shows F-region velocity vectors. Electron densities along two of the radar beams directed poleward along the magnetic meridian are shown in the second and third panels, altitude being shown along the left axis and magnetic latitude along the right axis. Ground magnetic observations are shown from BETT and FYKN approximately along the PFISR meridian. Pi2 pulsations from EAGLE are shown in the bottom panel. The time of the identified substorm onset is indicated by a dashed vertical line; the latitude of initial substorm brightening is identified by a star in the flow vector panel (based on Lyons et al., 2010a, 2010b).

roughly the same local time sector as the radar. A substorm is shown by magnetic dipolarization signatures observed by THEMIS (third panel), as well as by the ground magnetic field decrease (geographic north component Bx) from available Greenland magnetometers within the auroral zone and by the positive bay seen by the Canadian mid-latitude magnetometer STJ nearest the Greenland meridian. We estimated the substorm onset to be at ~0205 UT, a few minutes before the radar FOV was engulfed by the expansion phase E-region ionospheric density enhancement.

While some data are missing due to the low F-region densities within the polar cap that occur during solar minimum conditions, at several latitudes a substantial southeastward directed flow enhancement can be seen to initiate at 0157 UT, ~8 min prior to onset. This time, identified by a dotted line in the figure, is close to the average time before onset that Nishimura et al. (2010a) reported the intensification of a PBI (~5.5 min). The entire E-region FOV of the radar (Λ ~72.3° to 74.3°) was within the polar cap when the flow enhancement was first observed, and enhanced flows were observed up to the poleward edge of the radar F-region FOV (Λ ~73.5°). Thus, the flow enhancement gave enhanced plasma transport across polar cap field lines towards the plasma sheet, as first observed by de la Beaujardière et al. (1994)) for flows associated with PBIs. The flow enhancement extended to the equatorward boundary of the radar F-region FOV, and thus likely crossed the polar cap boundary at about that time. While the transition to plasma sheet E-region densities was equatorward of the radar E-region FOV at this time, the F-region flow enhancement is seen to extend ~2° equatorward of the E-region FOV, so the enhanced flows likely crossed the open-close field line boundary as observed by de la Beaujardière et al. (1994). These flows likely enhanced transport of plasma lying along polar cap field lines into the plasma sheet, and they were seen at a time and location appropriate for leading to the substorm onset.

A more and thorough evaluation of radar flows associated with substorm onset has recently been completed (Lyons et al., 2020a; Radar Observations of Flows Leading to Substorm Onset over Alaska, submitted to *J. Geophys. Res*). That analysis identified 9 events, including one studied in detail by Nishimura et al. (2014), for which a substorm auroral onset was identified within the FOV of the Poker Flat ASI 557.7 nm imager and within or just equatorward of the latitudinal coverage of the PFISR beams. PFISR flow vectors and available SuperDARN LOS flows are overlaid on selected full 557.7 nm images in Fig. 7 for a substorm with onset seen in the aurora at 0803:20 UT on November 21, 2012. THEMIS ASI images extend outward from the Poker Flat ASI FOV. Inserts show LOS flows along the PFISR beams overlaid on blowups of the images in the vicinity of the PFISR FOV. Since the ASI images have 12 s resolution whereas the radar integration time has been taken as 1min, the insert images are for two ASI time steps prior to the full images.

Initially (0800 UT panel), the flow vectors show westward flow as

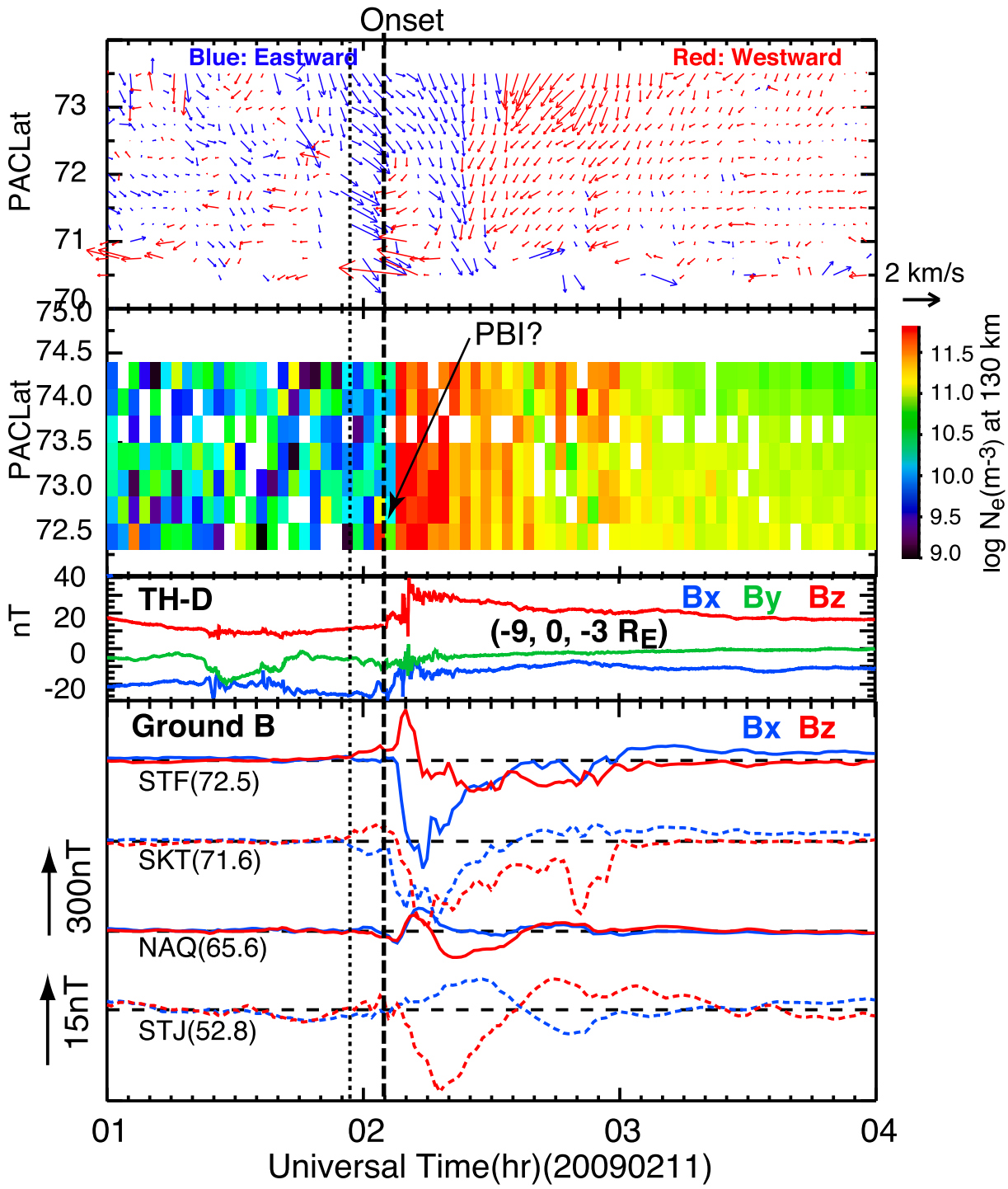

Fig. 6. Observations from a 3-hr interval during a Sondrestrom radar run on 11 February 2009. The top panel show the F-region vector as a function of magnetic laitude and UT. E-region densities at 130 km altitude as a function of magnetic latitude and UT are shown from each radar scan in the second panel. Values below and above ~3 × 10^{10} m^{-3} indicate polar cap and plasma sheet, respectively. The three magnetic field components from the THEMIS D spacecraft and Bx and Bz from available Greenland magnetometers ground stations and Canadian mid-latitude magnetometers nearest the Greenland meridian are shown in the bottom panels to identify onsets of Fig. 1. A vertical dashed line indicates the identified time of a substorm onset. The vertical dotted line identifies the initiation time of the observed pre-onset flow enhancement. A possible PBI signature is identified in E-region density panel. The THEMIS spacecraft location at the center of the time interval in the figure is given as (x,y,z) in GSM (based on Lyons et al., 2010a, 2010b).

expected from dusk cell convection, and the LOS flows are consistent with this inference. The aurora shows a typical east-west oriented arc very near the equatorward limit of the PFISR beam measurements, this arc being typical of the growth phase arc seen during a late substorm growth phase Then, in the 0801:40 UT insert, the LOS flows indicate a flow with a strong equatorward component intruding into the poleward portion of the PFISR beams (indicated by a yellow arrow), the equatorward flow also being shown by the two most poleward flow vectors. This flow had then intruded all the way to the growth phase arc at the next radar measurement time (0803:07 UT insert and 0803:32 UT full ASI mosaic). The flow was also seen by the western-most SuperDARN radar beam in the 0803:32 UT panel, and onset occurred during this

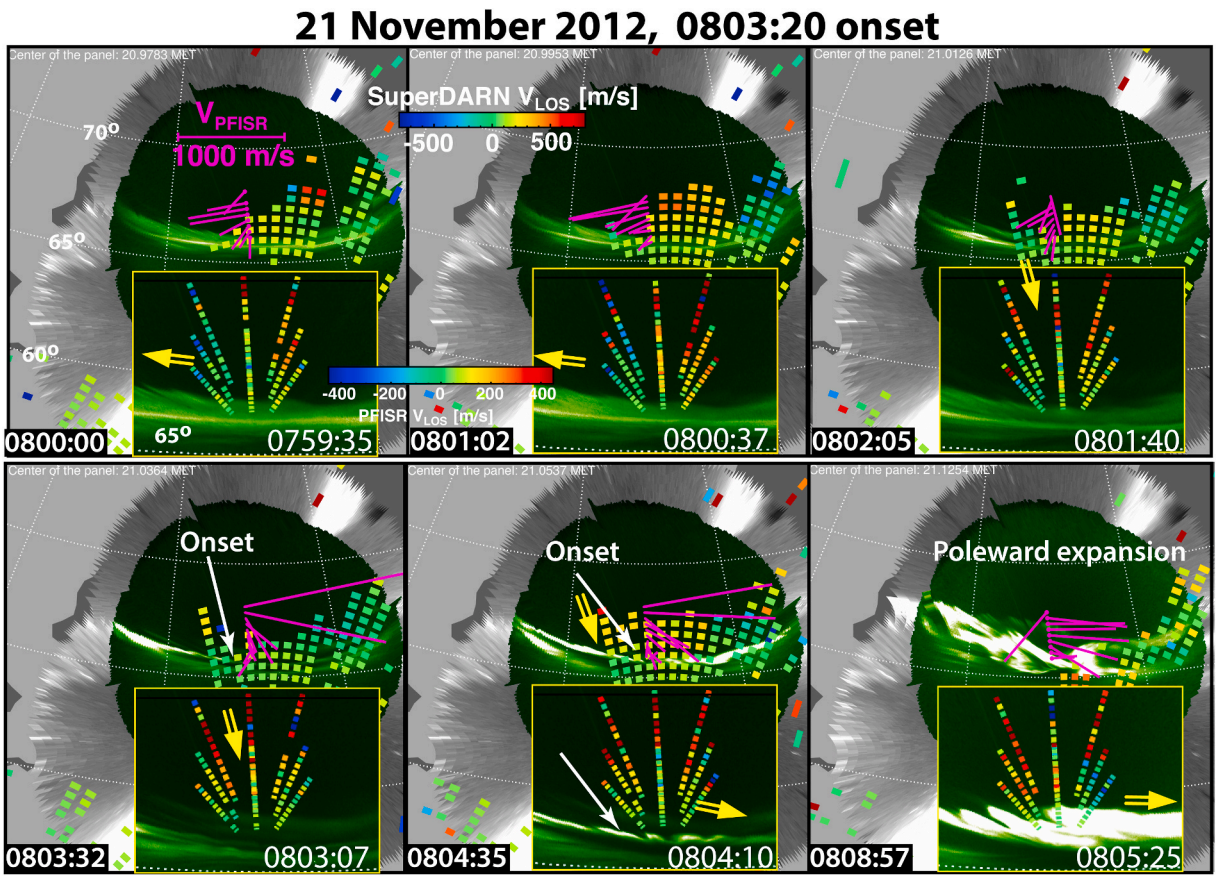

Fig. 7. 557.7 nm images from Poker color ASI, with THEMIS ASI image mosaics for the region surrounding the Poker image FOV for the 21 November 2012, 0803:20 onset. Images are shown every ~1 min, except for last image which was chosen to show the substorm poleward expansion ~4 min after the previous image. Objective flow vectors along the PFISR magnetic meridian are overlaid on the 557.7 images in each panel. LOS flows measured along the radar beams are shown overlaid on the lower image inserted into each of the 557.7 panels. These lower images are blowups of the 557.7 nm images over the region covered by the PFISR beams, and, to not repeat images, these images are for a slightly earlier time than the time of the full mosaics (except for the last panel). Yellow arrows in the 557.7 nm inserts are to illustrate flow directions inferred from the PFISR LOS flows and substorm auroral onset is identified by the white arrows (based on Lyons et al., 2020a, Radar Observations of Flows Leading to Longitudinal Expansion of Substorm Onset over Alaska, submitted to J. Geophys. Res).

radar measurement minute. The beginning of wave growth from the initial onset beading can been seen in the 0804:10 UT insert, with further wave growth seen in the 0805:25 UT insert. Furthermore, the onset was first seen just to the west of the PFISR meridian and just where the intruding flow channel was observed. The intruding flow continued during the next measurement minute as the auroral expansion started to develop, and the flow then turned eastward. Poleward expansion of the auroral activity is represented by the final full ASI image at 0808:57 UT. This was a thin auroral oval event, so it would be difficult to identify a streamer associated with the intruding flow channel. However, with the PFISR data, we see the flow channel very clearly heading to the onset location just before onset.

As noted above when discussing the example in Fig. 6, the flow channels that initiate substorm onset appear to come from polar cap flow channels that cross the auroral oval poleward boundary and enter the closed field line region of the auroral oval. This is as initially proposed by Nishimura et al. (2010a), based on the observation that the pre-onset substorm sequences as seen in the aurora start with a PBI. That PBIs are associated with flow channels that enter the auroral oval from the polar cap was clearly demonstrated in the first paper that identified the feature now known as PBIs (de la Beaujardière et al., 1994), and has been demonstrated in a number of subsequent studies (Lorentzen et al., 2004; Moen et al., 2007, p. 204; Pitkänen et al., 2013; Shi et al., 2012), including on a statistical basis by Zou et al. (2014). In the tail, these flows correspond to localized flow that crosses into the plasma sheet from the lobes, corresponding to an increase in the local reconnection rate (Blanchard et al., 1996). Evidence for such enhanced flows crossing from the lobe into the plasma sheet prior to substorm onset has been seen with the THEMIS spacecraft near the outer boundary of the plasma sheet (; Angelopoulos et al., 2008, 2009; Lyons et al., 2010b), and in the ionosphere with radars (Lyons et al., 2011) and from optical observation of F-region ionization patches and polar cap arcs (Nishimura et al., 2013a).

2. East-west alignment and expansion of transition to instability

Tail flow bursts are normally thought as being flow channels that extend radially but are narrow in azimuthal extent, as seen in MHD simulations of flow bursts (e.g., Birn et al., 2004)). If this were true when flow channels reached the inner plasma sheet, they could not account for the azimuthal alignment and spreading of the substorm onset instability. However, Rice Convection Model (RCM) modeling show a very clear longitudinal expansion of the reduced entropy plasma that comprises a plasma sheet flow channel as it extends to the inner plasma sheet (Wang et al., 2018; Jian Yang et al., 2014). This offers a viable explanation for why the onset instability initially extends, and then expands, longitudinally.

2.1. RCM-UCLA modeling

Fig. 8 shows results in the equatorial plane using the UCLA equilibrium version of the Rice Convection model (RCM-UCLA) of Wang et al.

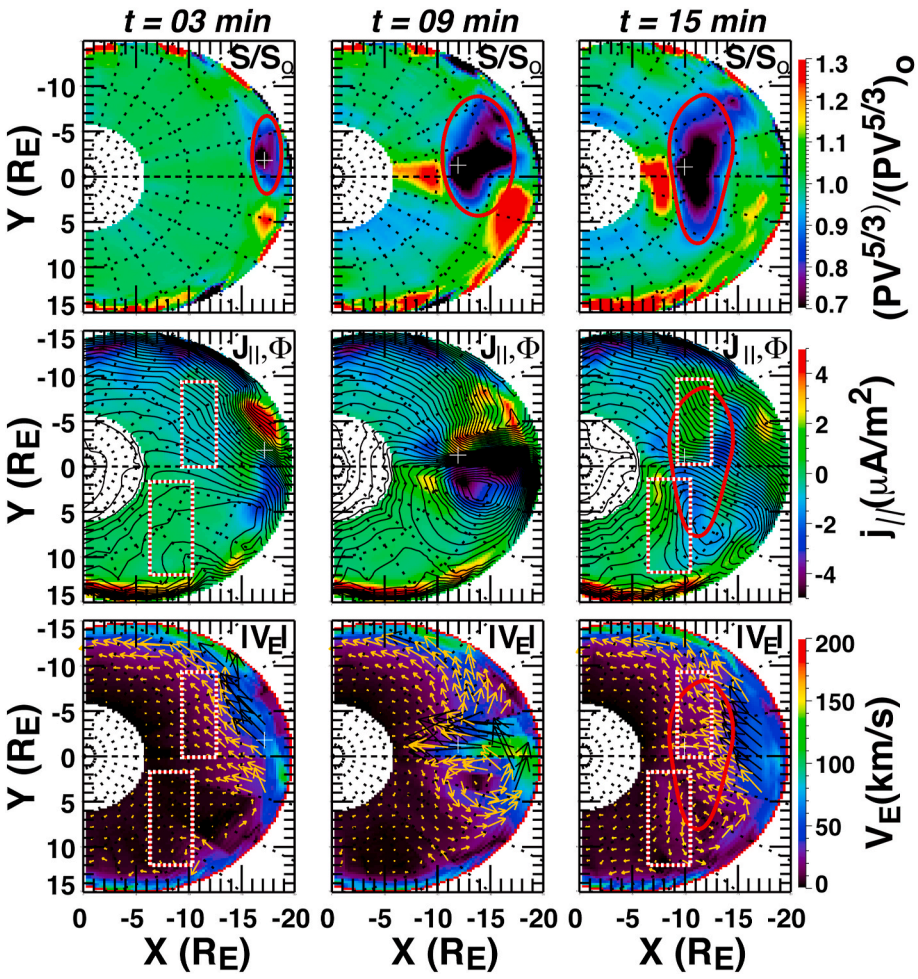

Fig. 8. Nightside RCM-UCLA results for times 3, 9, and 15 min after a meso-scale perturbation with a 1 h in MLT width was imposed on the RCM outer boundary that lead to bubble formation from energy-dependent magnetic drift. The top row shows the ratio of flux tube integrated entropy S to the integrated entropy S_o at t = 0. The middle row show field-aligned current density at the top of the ionosphere and equipotential contours with 2 kV separation, and the lower row should the electric field drift speed both color coded and as vectors. Crimson curves in the top row illustrate the approximate boundary of the expanding bubble for each of the three times, and the crimson curve from the top row at t = 15 min is copied onto the middle and lower rows. Red and white rectangles are drawn to help identify the locations for making the comparison between equipotentials and electric field drifts at t = 3 and t = 15 min based on (based on Wang et al., 2018).

(2018) for times 3, 9, and 15 min after a meso-scale perturbation with a 1 h in MLT width was imposed on the RCM outer boundary, which is near X = −20 R_E at midnight. Since the perturbation (Run 1 of Wang et al.) had a density decrease by a factor of 6 and a temperature increase by a factor of 6, the bubble was created by the divergence of the heat flux vector resulting from the higher magnetic drift speeds of the hotter plasma particles relative to those of the cooler background. Note that violation of plasma entropy conservation is a unavoidable consequence of magnetic drift, but is not allowed by ideal MHD models (See review, Lyons et al., 2009). As the bubble moves earthward, the lower energy ions tend to follow the electric field drift (along equipotentials, which are shown as the black contours in the middle row). However, the higher energy ions magnetic drift towards the duskside. As a result, entropy is not conserved along center of mass drift trajectories, and the bubble spreads in longitude and deepens as it moves earthward. The spreading is seen in the top row of Fig. 8, which shows the flux tube integrated entropy S normalized to the integrated entropy S_o at t = 0 ($S = PV^{5/3}$, where P is plasma pressure and V is flux tube volume), with a crimson curve illustrating the approximate boundary of the expanding bubble for each time. The gradient of S is typically tailward in the plasma sheet. However, the bubble spreading leads to an approximately azimuthal-aligned decrease in the tailward gradient in S at t = 15 min, a gradient change that expands azimuthally with time and is of the appropriate sign (e.g., Xing and Wolf, 2007) to give azimuthal expansion of the substorm onset instability.

FACs as mapped to the ionosphere as shown in the middle row of Fig. 1, downward currents being positive. An enhancement of the Region 1 and 2-sense FACs can be seen with the bubble as it moves earthward (t = 9 min), and these FACs become longitudinally broad Region 1 and Region 2-sense current enhancements that are associated with the azimuthal spread of the bubble after it approaches the subauroral region (t = 15 min). The enhanced Region 1-sense FACs at t = 15 min are approximately collocated with the bubble itself, as can be seen by comparing the FACS to the crimson curve that has been copied from the top row at t = 15 min onto the middle and lower rows of Fig. 8, whereas the enhanced Region 2 FACs are earthward of the bubble. (There additional more poleward FAC changes at t = 15 min are not considered here.)

The enhanced FACs are related to changes in the electric field, changes which maintain current continuity in the ionosphere. The electric field changes appear as azimuthal turnings of the flows as the flow channel moves earthward (t = 9 min) toward the inner plasma sheet. By t = 15 min on the dusk side, the change is an electric field enhancement that corresponds to significant enhancements in the sub-electron auroral region flows that are referred to as subauroral polarization streamers (SAPS) (e.g., Foster and Burke, 2002). On the dawnside, the electric field change is an enhancement that is more poleward, such an electric field enhancement giving strong flows that have recently been referred to as dawnside auroral polarization streams, or DAPS (Liu et al., 2020). Both of these flows occur in the regions of the enhanced downward FACs (Region 1 for SAPS, Region 2 forDAPS), where conductivities are substantially lower than in the upward FAC regions. These enhancements can be seen by comparing the electric equipotentials and the electric field drift velocities in the middle and bottom rows, respectively, at t = 3 and t = 15 min. Red and white rectangles in Fig. 1 are drawn to help identify the regions for making this

comparison. Also, comparison with the crimson curve, shows that the DAPS increase is within the plasma sheet bubble, while the SAPS increase is adjacent to the equatorward boundary of the bubble.

The azimuthal turning of the flows in the plasma sheet at t = 9 min is similar to that seen by Ogasawara et al. (2011) within the plasma sheet during substorm azimuthal expansion and offers an explanation for the connection between azimuthal flows and adjacent streamers as suggested by Haerendel (2015), and the current and flow enhancements at t = 15 min are very much like those seen from the ground by Zou et al. (2009) during the azimuthal development of the substorm expansion phase. These correspondences indicate the plausibility that azimuthal expansion of the substorm onset instability is related to the expansion of incoming reduced entropy bubbles. Note that the spreading and flows are beyond the capabilities of current MHD simulations of bubbles (e.g., Birn et al., 2004).

2.2. Observations

Since the electric potentials associated with a bubble give current continuity and map from ionosphere to the magnetosphere, bubble-related electric field enhancements within the ionosphere have the potential to be used of a signature of the longitudinal expansion of bubble. This provides a test of the RCM model predictions for azimuthal expansion of a bubble in the inner plasma sheet, and in particular the idea that the substorm onset instability initially extends, and then expands, longitudinally because the instability is triggered by the low entropy plasma of an incoming flow burst. For example, ground radar observations have previously shown SAPS enhancements following auroral streamers and their associated flow channels in the absence of substorms (Gallardo-Lacourt et al., 2017; Lyons et al., 2015; Makarevich et al., 2011), and DAPS enhancements can be inferred from the connection of the formation of dawnside, auroral omega bands to aurora streamers (Henderson et al., 2002) and to strong DAPS flows (Liu et al., 2018). These are both consistent with the RCM results.

Lyons et al. (2020b) (Radar Observations of Flows Leading to Longitudinal Expasion of Substorm Onset over Alaska, submitted to J. Geophys. Res) analyzed several substorm events for consistence with the RCM modeling results. Fig. 9 shows observations from a quite fortunate event on 15 March 2013 that occurred where the radar observations allowed all the flow features associated with on incoming bubble to be seen. The format in the upper panels is the same as in Fig. 5, and the lower panels of show a sequence Poker 630 nm images for this event with plasma densities along each radar beam overlaid of the images. LOS flows from available SuperDARN radar echoes are shown in the 557.7 nm and 630 nm image panels, the spatial extend of the coverage shown being larger in the 630 nm panels. The incoming flow channel leading to the onset was seen by SuperDARN adjacent to a polar cap arc, and is identified in the 1043:45 and 1050: 25 UT 630 nm panels of Fig. 9. In the 1052:05 and 1055:25 UT 630 nm panels, the SuperDARN echoes show very clearly a flow increase that is likely SAPS, since it is equatorward of detectable aurora. The increase is first seen just after onset but before auroral poleward expansion, and thus it is as expected from a pre-onset flow channel that led to onset. Additionally, an increase can be seen in DAPS flows as onset spread eastward into the PFISR FOV, and this increase also was first seen before significant auroral poleward expansion. (There is also a sharp transition to westward flows at the poleward boundary of the DAPS flows. This transition appears to correspond to the auroral poleward boundary, and the more poleward SuperDARN LOS flows are consistent with flows being westward within the nearby polar cap.)

3. Post-onset flow channels: cause of substorm current wedge and classical substorm onset signatures

The concept of a substorm (initially referred to as a magnetic bay) was initially based on ground magnetometer observations (Akasofu, 1968; Chapman, 1956; Silsbee and Vestine, 1942, and references therein). Its onset was later defined and identified by the initial auroral brightening (Akasofu, 1964). However, the auroral onset has a general association with sudden H increases (positive bays) (e.g., Iijima and Nagata, 1972) and with suddenly enhanced Pi2 pulsations seen by ground magnetometers at mid-to-low latitudes (e.g., Rostoker, 1968; Sakurai and Saito, 1976; Lester et al., 1983), and with sudden negative changes of the ground H component at auroral latitudes (i.e., initiation of magnetic bays) (e.g., Akasofu and Meng, 1969; Nishida and Kokubun, 1971). The above H changes are a manifestation of the three-dimensional current system that is referred to as the substorm current wedge (SCW) (Bonnevier et al., 1970; McPherron et al., 1973), which had been generally viewed as a single current system that expands azimuthally with time during the substorm expansion phase (e.g., Nagai, 1982, 1987). Pi2 enhancements have been attributed to the current enhancement leading to the substorm current wedge (Baumjohann and

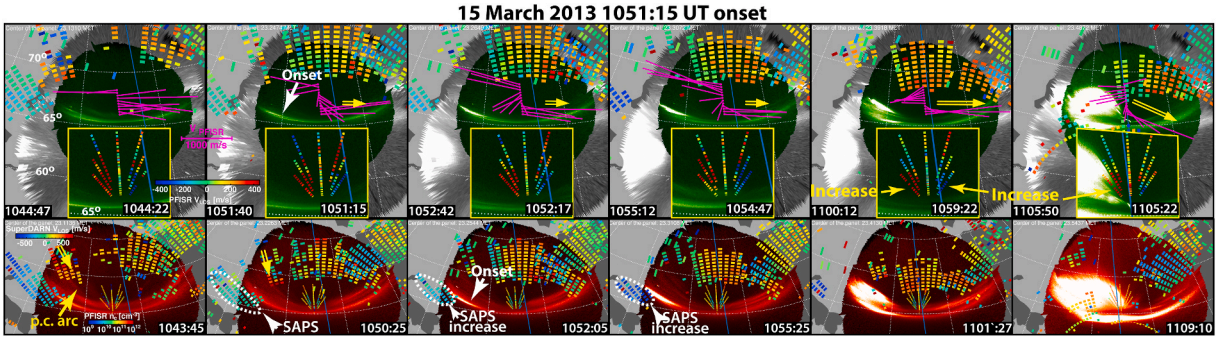

Fig. 9. The upper panels of each row show 557.7 nm images from the Poker color ASI, with THEMIS ASI image mosaics for the region surrounding the Poker image FOV for the 1051:15 onsets on 15 March 2012. Images are show at times selected to illustrate features of interest. Objective flow vectors along the PFISR magnetic meridian are overlaid on the 557.7 images in each panel. LOS flows measured along the radar beams are shown overlaid on the lower image inserted into each of the 557.7 panels. These lower images are blowups of the 557.7 nm images over the region covered by the PFISR beams, and, to not repeat images, these images are for a slightly earlier time than the time of the full mosaics. The lower panels of each row show a sequence of Poker 630 nm images for this event. In case a reader might be interested, the plasma densities along each radar beam overlaid of the images. LOS flows from available SuperDARN radar echoes are shown in the 5577 nm and 630 nm images panels, the spatial extend of the coverage shown being larger in the 630 nm panels because of the larger spatial FOV of the 630 nm images due to their higher emission altitude (taken to be 120 km for the 557.7 nm and 210 km for the 630.0 nm). Yellow arrows in the 557.7 nm insert are to illustrate flow directions inferred from the PFISR LOS flows, substorm auroral onset is identified by the white arrows, and yellow arrows in the 630 nm panels identify an equatorward moving polar cap patch (Based on Lyons et al., 2020b, Radar Observations of Flows Leading to Longitudinal Expasion of Substorm Onset over Alaska, submitted to *J. Geophys. Res*).

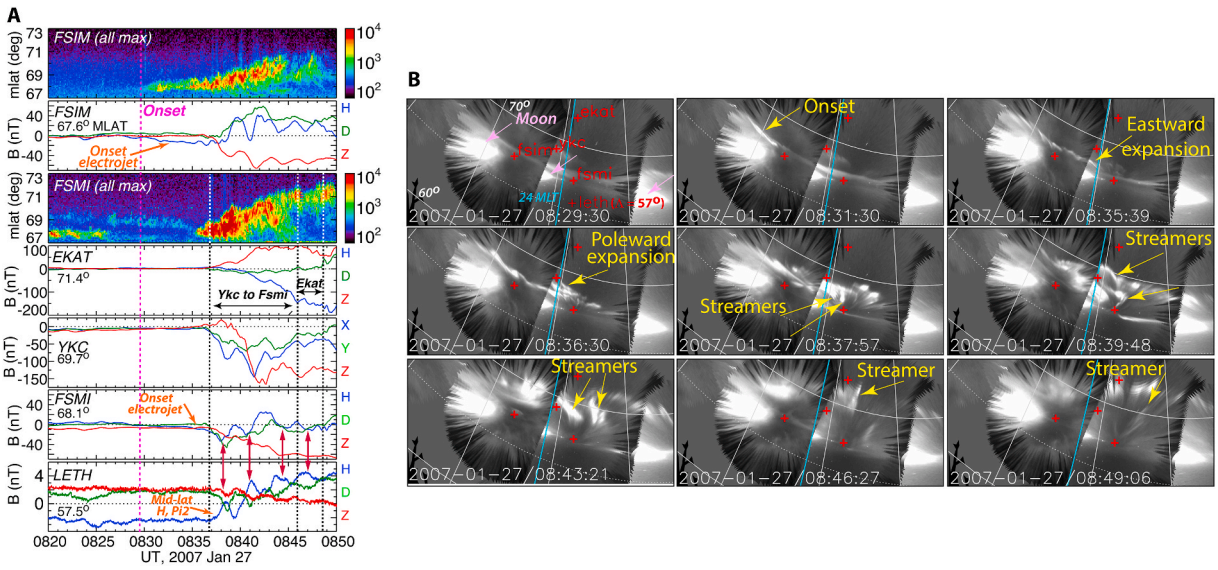

Fig. 10. (A) Keograms of the maximum auroral intensity over all measured longitudes from the FSIM and FSMI ASIs and the three components of the ground magnetic field from the stations identified by the red plus signs in Figure (B), covering the time interval of the 2007 January 27 event. "All max" means that each data point in the keogram is from the longitude having maximum intensity, all measured longitudes being included. The dashe vertical magenta line identifies substorm onset; vertical black dotted lines give the start and end times of intervals of streamers in the vicinity of the identified ground stations. Orange arrows identify the very weak and gradual H decreases at FSIM and FSMI between the times of onset and streamer formation that indicate the formation of a very weak westward electrojet. (B) Selected mergers of the auroral images from the THEMIS ASIs for the time interval of the of the 2007 January 27 event. Yellow arrows and associated text identify the main auroral features discussed in the text. Red plus signs (text) give the locations (names) of the gound magnetometer stations used in Fig. 10A. The cyan line marks magnetic midnight, and longitude lines are space 1 h in MLT apart. Moonlight contamination is identified in the first panel (based on Lyons et al., 2013a).

Glaβmeier, 1984; Lester et al., 1983)]. Due to their general association with the auroral onset, the onset of the Pi2 enhancements and of the mid/low- and auroral-latitude H changes have all been viewed as signatures not only of the initiation of current-wedge enhancement, but also of substorm onset.

Formation of the SCW has often been viewed as a fundamental aspect of the substorm onset process and critical for understanding the substorm expansion phase (Lyons, 1996). Traditionally, it has been viewed as a large-scale, wedge-shaped current system (Chu et al., 2015; Gelpi et al., 1987; Liang et al., 2018; McPherron et al., 1973). On the other hand, a number of studies have reported signatures of multiple localized currents (wedgelets) that are separated azimuthally by hundreds of km (Kauristie et al., 2000; Liu et al., 2015; Lyons et al., 2012; Palin et al., 2015; Pytte et al., 1976; Sergeev, 1974). Particularly clear are observations multispacecraft observations from perigee passes of Cluster spacecraft during a substorm by Forsyth et al. (2014). As the spacecraft traveled east-west azimuthally above the substorm auroral region, the SCW was seen to be comprised of significant azimuthal substructures on scales of 100 km at altitudes of 4000–7000 km. It now seems clear that the SCW is built up by multiple wedge-type currents located across the longitude range of the substorm bulge, and Liu et al. (2015) showed that each of these wedgelets are drvien by flow bursts in the tail that contain stronger magnetic field within them (referred to as "dipolarizing flux bundles") than does the surrounding plasma.

As with flow bursts in general, SCW wedgelets should be associated with auroral streamers; however, the initial aurora beading is not comprised of auroral streamers so that it should not be associated with the onset of the SCW. We would expect SCW formation, and its initial signatures that are traditionally used to identify substorm, to be post-onset features that occur once the non-linear evolution of the auroral bead waves leads to streamers (Keiling et al., 2009; Lyons et al., 2013a; Rae et al., 2009). The corresponding fast flows within the plasma sheet can then initiate current wedge formation and the associated substorm magnetic signatures on the ground and dipolarization within the near-Earth plasma sheet. Because the initial streamers after substorm onset develop from the onset waves within the plasma sheet, the initial streamers could be associated with reconnection signatures seen within the plasma at X_{gsm} at a near-Earth neutral line, which occurs at distances of $\sim -20\ R_E$ soon after onset (e.g., Machida et al., 2009; Nishimura et al., 2013b).

That the ground magnetic responses to SCW formation traditionally viewed as signatures of substorm onset may be related to post-onset auroral streamers rather than to substorm onset was considered in Lyons et al. (2012, 2013a). An example of the ground magnetic and ASI observations they evaluated is given in Fig. 10. Keograms in Fig. 10A give the maximum auroral intensity over all measured longitudes (to show all aurora that may contribute to the local ground magnetic field) from a more western ASI (FSIM) and a more eastern ASI (FSMI) station. Selected snapshots of combined ASI images from stations covering the onset and subsequent expansion phase activity are shown in Fig. 10B. The first panel of Fig. 10B shows the location of the stations for which magnetic field data are shown in Fig. 10A. Substorm onset is determined from the auroral brightening at 0829:30 UT, and subsequent slow auroral brightening and poleward expansion are clearly seen in the FSIM keogram. The intensified onset auroral arc is identified in the second panel of Fig. 10B, and the beading along the onset arc is clearly seen in the subsequent (0835:39 UT) image as the onset aurora continued and expanded eastward to FSMI.

Substantial poleward expansion initiated at ~0836 UT, and after that time, streamers started to evolve and move equatorward from the auroral poleward boundary. Several of the most prominent ones are identified in the last 5 panels of Fig. 10B. The first vertical black dotted line in Fig. 1A identifies the time when the sequence of auroral streamers started to develop in the longitude region from near YKC to FSMI. This continued for ~9 min, as indicated by the second vertical dashed line, and was followed for a few more minutes by streamers in approximately the same longitude region, but emanating from more poleward latitudes closer to that of EKAT in association with the continued poleward expansion of the aurora.

Following the auroral onset, but before the onset of the streamers, the magnetometer observations show only very weak and gradual H decreases at FSIM and FSMI following the onset. This would indicate the

formation of a very weak westward electrojet. No mid-latitude positive bay or Pi2 enhancement was seen. Traditional magnetic onset signatures were then seen at the time of the formation of the streamers, ~7 min after auroral onset, the signatures including the sharp drop in the H component at YKC, the sharp increases (decreases) in the Z component at the lower (higher) latitude auroral zone station FSIM (EKAT), and the mid-latitude positive bay and Pi2 pulsation initiation. The strongest H decreases moved poleward from YKC to EKAT as the streamer initiation location moved poleward, consistent with these decreases being a response to the expansion phase streamers.

It is clear that the ground magnetic features that are traditionally viewed as signatures of substorm onset, and of significant current wedge formation, were all associated with the post-onset streamers, the delay from onset in the events considered in Lyons et al. (2013a, 2013b) varying from 1 to 10 min. For all events, the onset of streamers was at the time of the onset of the ground magnetic signatures and the largest H decreases where located in the vicinity of the streamers. This is all consistent with the substorm current wedge developing by a series of tail flow bursts, which can be referred to as wedgelets, and are seen in the ionosphere by auroral streamers.

While not noticed in the above papers, an interesting feature can be seen by comparing the H decreases at FSMI with the H increases seen at the subauroral station LETH, about 10° equatorward of FSMI and along almost the same magnetic meridian. This is indicated by the vertical maroon arrows near the bottom of Fig. 10A. Each H decrease at FSMI, which are responses to individual streamers and their associated flow channel, has a 1-to-1 correspondence with and H increase at LETH (and also with the H decreases at the more poleward auroral station YKC). This indicates that the H increases, which comprise the traditional substorm Pi2 pulsations, are not is fact a wave, but are the response to individual flow channels near that meridian. The field-aligned currents with each flow channel each give an elemental incremental increase of the H component at LETH, and each acts to build up the midlatitude positive bay and thus the large-scale substorm current wedge.

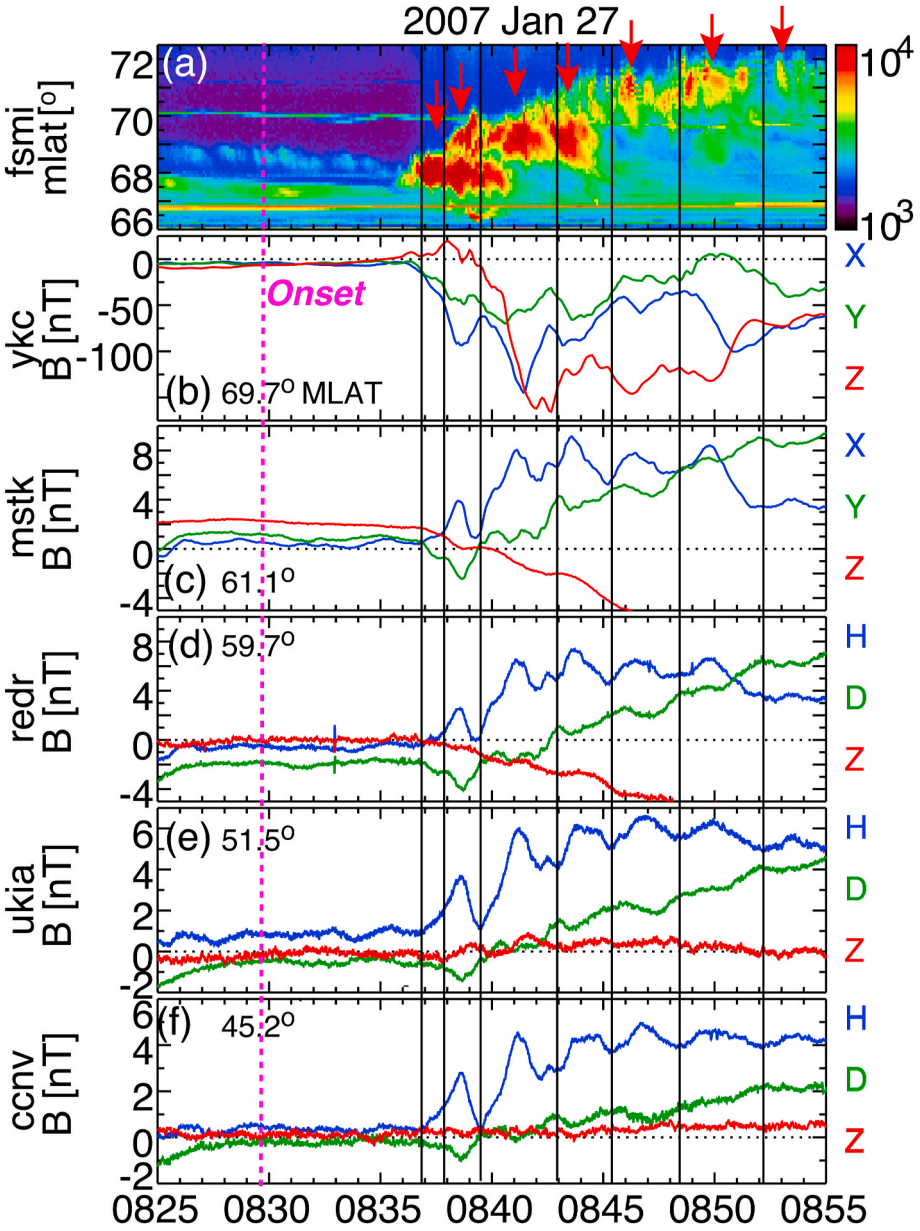

Fig. 11. FSMI auroral keograms and magnetometer data during the ~0830 UT substorm on 27 January 2007. Three components of ground magnetometer data are shown from stations approximately along the YKC magnetic meridian. The dashed magenta line shows the auroral onset time. The solid black vertical lines mark initiations of each Pi 2 pulse (based on Nishimura et al., 2012a, 2012b).

This feature was noticed and examined in detail in Nishimura et al. (2012a, 2012b). Fig. 11 repeats the auroral keogram from FSMI from Fig. 10A, but with its color scale adjusted so as to emphasize the more intense auroral streamers and inclusion of observations only from near the central meridian of the FOV (to see local auroral modulation). The YKC magnetometer is repeated, and is shown with 4 ground magnetic field measurements from 4 progressively lower latitude stations, all along approximately the same magnetic meridian. After ~0836-37 UT (first black vertical line), the auroral intensity during the poleward expansion seen by the FSMI ASI shows quasi-periodic intensifications as marked by red arrows in Fig. 11a. Each of these is a separate intensification occurring near or slightly poleward of the poleward edge of the pre-existing auroral bulge, leading to a stepwise poleward expansion of the expansion-phase aurora. Each intensification led to an equatorward-propagating auroral streamer some of which are identified in Fig. 10B.

As indicated by the vertical lines in Fig. 11, the initiation of each expansion-phase auroral intensifications is correlated remarkably with initiations of individual Pi2 pulses at all the mid-latitude stations. Each Pi 2 pulse started to rise with each auroral intensification without a significant time lag. As noted above, the negative bay in the H component in the auroral zone at YKC located near the streamers (Fig. 10B) oscillated in anti-phase with the midlatitude Pi 2. The coherence of the expansion-phase intensifications, and the midlatitude and auroral zone Pi 2 indicates that these three phenomena were driven by flow channels comprising the SCW wedgelets. Note that we focus primarily on initiation of H pulses and do not discuss the timing of the peaks, since peak timing depends not only on auroral intensity but also on azimuthal propagation and orientation of the streamers relative to an observing ground magnetometer station.

4. Summary and future directions

As described here, and schematically summarized in Fig. 12, our research has shown the following about the substorm expansion phase and where we believe there are important outstanding questions.

1. Substorm onset occur within the outer portion of the growth phase partial ring current, which equates to the inner region of the proton plasma sheet, and maps to the equatorial plane to where the magnetic field transitions from being highly stretched to more dipolar.
2. The auroral beading at onset and subsequent growth of these onset waves indicate that substorm onset occurs as the result of an abrupt transition from a stable to unstable state along field lines of the inner plasma sheet. This is also supported by the large-amplitude electric oscillations that are seen in the ionosphere to initiate at the onset of the auroral beading.
3. The unstable region is azimuthally aligned in the ionosphere and expands azimuthally after initial onset.
4. The observation of streamers leading to onset indicates that the transition to instability occurs as a result of an intrusion of a low-entropy flow burst/channel (i.e., a plasma bubble) to the inner plasma sheet, and this is strongly supported by radar observations showing the ionospheric mapping of incoming flow channel directed to the time and location of onset.
5. Such flow bursts are marked in the auroral oval by the initiation of a PBI that evolves into an auroral streamer. Plasma flows associated with these and other PBIs and streamers appear to generally be associated with enhanced reconnection at the distant tail neutral line, the reconnection being triggered by an incoming flow channel from the polar cap.

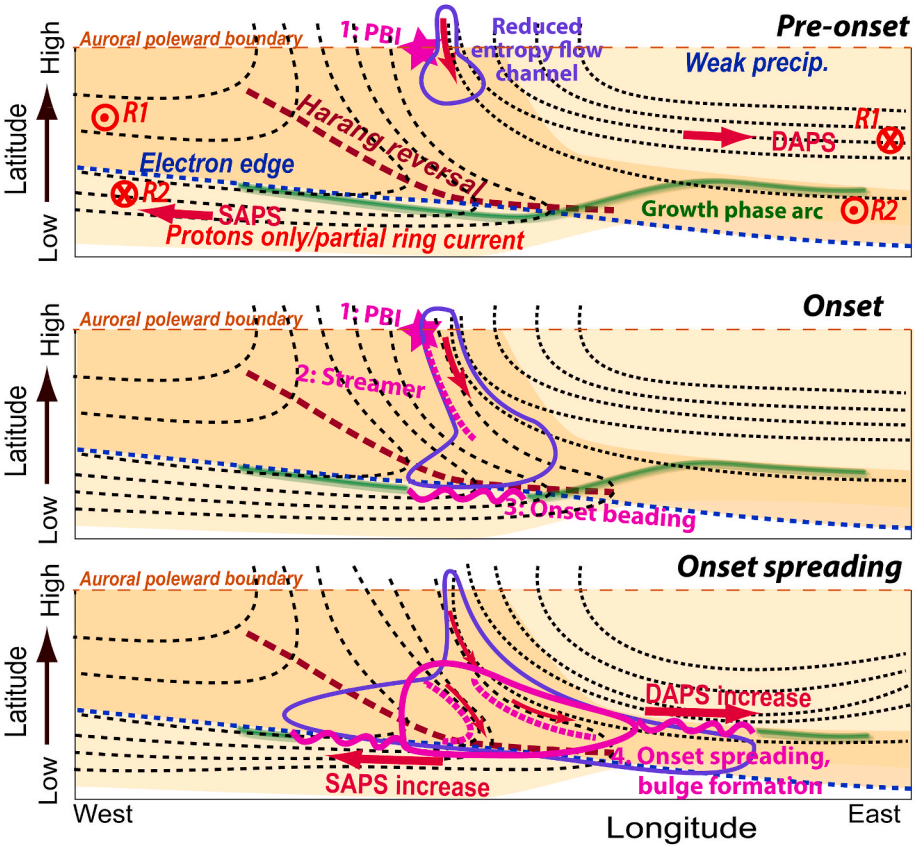

Fig. 12. Schematic summary of the substorm onset sequence envisoned in this review.

6. It is reasonable that the plasma sheet flow channels trigger the onset instability by bringing reduced entropy plasma to the inner plasma sheet and abruptly changing the entropy distribution in the inner plasma sheet. Identification of the onset instability is crucial outstanding question. It could perhaps be related to a local reversing of sign of the radial gradient of entropy, leading to a ballooning type of instability such as the kinetic ballooning/interchange instability found by Pritchett et al. (2014) using three-dimensional electromagnetic particle-in-cell simulations.
7. The onset instability is azimuthally aligned and expands azimuthally as a result of the azimuthal expansion of the incoming low entropy plasma bubble that initiates the instability. The azimuthal expansion occurs as the bubble moves earthward, the lower energy ions tending to follow the electric field drift towards the dawn side, while the higher energy ions magnetic drift towards the duskside. As a result, entropy is not conserved along center of mass drift trajectories, and the bubble spreads in longitude and deepens as it moves earthward. This crucial aspect of the plasma sheet bubbles and substorm onset is beyond the limits of ideal MHD models.
8. The growth of the onset waves leads to streamers. How this occurs is another major outstanding question, but the first streamers could initiate within the plasma sheet ~20 R_E downtail, the region where reconnection has been inferred to occur soon after onset. It is likely that streamers and their associated reconnection initiate at the distant tail neutral line once the expansion phase auroral reaches the auroral poleward boundary. It is not known whether or not the distant tail neutral line is same one that existed before onset, or results from the tailward expansion of a nearer Earth reconnection region that forms as a result of the growth of the onset waves.
9. The SCW wedge builds up from a sequence of longitudinally localized flow burst regions (wedgelets) that dipolarize the local magnetic field, these regions also giving rise to traditional substorm onset signatures on the ground, namely auroral zone H bays and mid-latitude positive H bays and Pi2 pulsations.
10. There are other potentially very important consequences of substorm expansion phase flow channels for which there is now some evidence but which require further investigation. These may strongly affect the longitudinal extent, polar extension, and duration of substorm expansion phase activity and include:

a. Are polar cap flow channels directed toward the poleward boundary of the nightside auroral oval important in controlling poleward expansion and duration of post-substorm onset auroral activity as indicated by the observations in Lyons et al. (2011)

b. The westward traveling surge initiates later than does the longitudinal expansion of the brightening of the onset arc, and typically develops after auroral activity reaches the polar cap boundary and then protrudes into the pre-existing polar cap. Do polar cap flow channels feed cold plasma from the open polar cap field lines into the westward traveling surge and thus play a critical role in surge initiation, westward propagation, and poleward expansion as indicated by the observations of Lyons et al. (2013b).

c. What is the role of multiple flow channels in controlling the development of substorm expansion? In particular, can there be more than one flow channel that sets of the substorm onset instability and contributes to the longitudinal expansion of the substorm expansion phase? These could be two flow channels that are separated in longitude that intrude to the inner plasma sheet at the time of onset, or the result of low channels that intrude after onset but are outside the longitude range of expansion phase activity at their time of intrusion.

Declaration of competing interest

The authors declare that they have no known competing financial interests or personal relationships that could have appeared to influence the work reported in this paper.

Acknowledgements

Work at UCLA has been supported by NSF grant 1401822 and AFOSR FA9559-16-1-0364, at Boston University by AFOSR FA9559-16-1-0364, NASA 80NSSC18K0657, and NSF AGS-1907698. The THEMIS ASI data is from http://themis.ssl.berkeley.edu/themisdata/.

References

Akasofu, S.-I., 1964. The development of the auroral substorm. Planet. Space Sci. 12 (4), 273–282. https://doi.org/10.1016/0032-0633(64)90151-5.
Akasofu, S.-I., Meng, C.-I., 1969. A study of polar magnetic substorms. J. Geophys. Res. 74 (1), 293–313. https://doi.org/10.1029/JA074i001p00293.
Akasofu, Syun-Ichi, 1968. Polar and Magnetospheric Substorms, vol. 11. Springer Netherlands, Dordrecht. https://doi.org/10.1007/978-94-010-3461-6.
Angelopoulos, V., 2008. The THEMIS mission. Space Sci. Rev. 141 (1–4), 5–34. https://doi.org/10.1007/s11214-008-9336-1.
Angelopoulos, Vassilis, McFadden, J.P., Larson, D., Carlson, C.W., Mende, S.B., Frey, H., et al., 2008. Tail reconnection triggering substorm onset. Science 321 (5891), 931–935. https://doi.org/10.1126/science.1160495.
Angelopoulos, Vassilis, McFadden, J.P., Larson, D., Carlson, C.W., Mende, S.B., Frey, H., et al., 2009. Response to comment on "tail reconnection triggering substorm onset. Science 324 (5933), 1391. https://doi.org/10.1126/science.1168045.
Baumjohann, W., Glaßmeier, K.-H., 1984. The transient response mechanism and Pi2 pulsations at substorm onset—review and outlook. Planet. Space Sci. 32 (11), 1361–1370. https://doi.org/10.1016/0032-0633(84)90079-5.
de la Beaujardière, O., Lyons, L.R., Ruohoniemi, J.M., Friis-Christensen, E., Danielsen, C., Rich, F.J., Newell, P.T., 1994. Quiet-time intensifications along the poleward auroral boundary near midnight. J. Geophys. Res. 99 (A1), 287–298. https://doi.org/10.1029/93JA01947.
Birn, J., Raeder, J., Wang, Y.L., Wolf, R.A., Hesse, M., 2004. On the propagation of bubbles in the geomagnetic tail. Ann. Geophys. 22 (5), 1773–1786. https://doi.org/10.5194/angeo-22-1773-2004.
Blanchard, G.T., Lyons, L.R., de la Beaujardière, O., Doe, R.A., Mendillo, M., 1996. Measurement of the magnetotail reconnection rate. J. Geophys. Res. 101 (A7), 15265–15276. https://doi.org/10.1029/96JA00414.
Bonnevier, B., Boström, R., Rostoker, G., 1970. A three-dimensional model current system for polar magnetic substorms. J. Geophys. Res. 75 (1), 107–122. https://doi.org/10.1029/JA075i001p00107.
Chapman, S., 1956. The morphology of geomagnetic storms and bays: a general review. Vistas Astron. 2, 912–928. https://doi.org/10.1016/0083-6656(56)90016-2.
Cheng, C.Z., Lui, A.T.Y., 1998. Kinetic ballooning instability for substorm onset and current disruption observed by AMPTE/CCE. Geophys. Res. Lett. 25 (21), 4091–4094. https://doi.org/10.1029/1998GL900093.
Chu, X., McPherron, R.L., Hsu, T.-S., Angelopoulos, V., Pu, Z., Yao, Z., et al., 2015. Magnetic mapping effects of substorm currents leading to auroral poleward expansion and equatorward retreat. J. Geophys. Res.: Space Phys. 120 (1), 253–265. https://doi.org/10.1002/2014JA020596.
Deehr, C., Lummerzheim, D., 2001. Ground-based optical observations of hydrogen emission in the auroral substorm. J. Geophys. Res.: Space Phys. 106 (A1), 33–44. https://doi.org/10.1029/2000JA002010.
Donovan, E., Liu, W., Liang, J., Spanswick, E., Voronkov, I., Connors, M., et al., 2008. Simultaneous THEMIS in situ and auroral observations of a small substorm. Geophys. Res. Lett. 35 (17), L17S18. https://doi.org/10.1029/2008GL033794.
Donovan, E.F., Mende, S., Jackel, B., Syrjäsuo, M., Meurant, M., Voronkov, I., Angelopoulos, V., Connors, M., 2006. The azimuthal evolution of the substorm expansive phase onset aurora. University of Calgary, Alberta, Canada, pp. 55–60.
Dubyagin, S., Sergeev, V., Apatenkov, S., Angelopoulos, V., Nakamura, R., McFadden, J., et al., 2010. Pressure and entropy changes in the flow-braking region during magnetic field dipolarization. J. Geophys. Res. 115 https://doi.org/10.1029/2010JA015625.
Forsyth, C., Fazakerley, A.N., Rae, I.J., Watt, C.E.J., Murphy, K., Wild, J.A., et al., 2014. In situ spatiotemporal measurements of the detailed azimuthal substructure of the substorm current wedge. J. Geophys. Res.: Space Phys. 119 (2), 927–946. https://doi.org/10.1002/2013JA019302.
Foster, J.C., Burke, W.J., 2002. SAPS: a new categorization for sub-auroral electric fields. Eos, Trans. Am. Geophys. Union 83 (36), 393–394. https://doi.org/10.1029/2002EO000289.
Frey, H.U., 2010. Comment on "Substorm triggering by new plasma intrusion: THEMIS all-sky imager observations" by Y. Nishimura et al. J. Geophys. Res.: Space Phys. 115 (A12), A12232. https://doi.org/10.1029/2010JA016113.
Gallardo-Lacourt, B., Nishimura, Y., Lyons, L.R., Zou, S., Angelopoulos, V., Donovan, E., et al., 2014a. Coordinated SuperDARN THEMIS ASI observations of mesoscale flow bursts associated with auroral streamers. J. Geophys. Res.: Space Phys. 119 (1), 142–150. https://doi.org/10.1002/2013JA019245.
Gallardo-Lacourt, B., Nishimura, Y., Lyons, L.R., Ruohoniemi, J.M., Donovan, E., Angelopoulos, V., et al., 2014b. Ionospheric flow structures associated with auroral beading at substorm auroral onset. J. Geophys. Res.: Space Phys. 119 (11), 9150–9159. https://doi.org/10.1002/2014JA020298.

Gallardo-Lacourt, B., Nishimura, Y., Lyons, L.R., Mishin, E.V., Ruohoniemi, J.M., Donovan, E.F., et al., 2017. Influence of auroral streamers on rapid evolution of ionospheric SAPS flows. J. Geophys. Res.: Space Phys. 122 (12), 406–412. https://doi.org/10.1002/2017JA024198, 420.

Gelpi, C., Singer, H.J., Hughes, W.J., 1987. A comparison of magnetic signatures and DMSP auroral images at substorm onset: three case studies. J. Geophys. Res.: Space Phys. 92 (A3), 2447–2460. https://doi.org/10.1029/JA092iA03p02447.

Haerendel, G., 2011. Six auroral generators: a review. J. Geophys. Res.: Space Phys. 116 (A1) https://doi.org/10.1029/2010JA016425 n/a–n/a.

Haerendel, G., 2015. Substorm onset: current sheet avalanche and stop layer. J. Geophys. Res.: Space Phys. 120 (3), 1697–1714. https://doi.org/10.1002/2014JA020571.

Henderson, M.G., Reeves, G.D., Murphree, J.S., 1998. Are north-south aligned auroral structures an ionospheric manifestation of bursty bulk flows? Geophys. Res. Lett. 25 (19), 3737–3740.

Henderson, M.G., Kepko, L., Spence, H.E., Connors, M., Sigwarth, J.B., Frank, L.A., singer, H.J., 2002. The evolution of north-south aligned auroral forms into auroral torch structures: the generation of omega bands and ps6 pulsations via flow bursts. In: Winglee, R.M. (Ed.), Sixth International Conference on Substorms. The University of Washington, Seattle, pp. 169–174.

Iijima, T., Nagata, T., 1972. Signatures for substorm development of the growth phase and expansion phase. Planet. Space Sci. 20 (7), 1095–1112. https://doi.org/10.1016/0032-0633(72)90219-X.

Kalmoni, N.M.E., Rae, I.J., Murphy, K.R., Forsyth, C., Watt, C.E.J., Owen, C.J., 2017. Statistical azimuthal structuring of the substorm onset arc: implications for the onset mechanism. Geophys. Res. Lett. 44 (5), 2078–2087. https://doi.org/10.1002/2016GL071826.

Kauristie, K., Sergeev, V.A., Kubyshkina, M., Pulkkinen, T.I., Angelopoulos, V., Phan, T., et al., 2000. Ionospheric current signatures of transient plasma sheet flows. J. Geophys. Res.: Space Phys. 105 (A5), 10677–10690. https://doi.org/10.1029/1999JA900487.

Keiling, A., Angelopoulos, V., Runov, A., Weygand, J., Apatenkov, S.V., Mende, S., et al., 2009. Substorm current wedge driven by plasma flow vortices: THEMIS observations. J. Geophys. Res. 114, 11. https://doi.org/10.1029/2009JA014114.

Lester, M., Hughes, J.W., Singer, H.J., 1983. Polarization patterns of Pi 2 magnetic pulsations and the substorm current wedge. J. Geophys. Res. 88 (A10), 7958–7966. https://doi.org/10.1029/JA088iA10p07958.

Liang, J., Donovan, E., Gillies, D., Spanswick, E., Connors, M., 2018. Proton auroras during the transitional stage of substorm onset. Earth Planets Space 70 (1), 126. https://doi.org/10.1186/s40623-018-0899-0.

Liang, J., Donovan, E.F., Liu, W.W., Jackel, B., Syrjäsuo, M., Mende, S.B., Frey, H.U., Angelopoulos, V., Connors, M., 2008. Intensification of preexisting auroral arc at substorm expansion phase onset: wave-like disruption during the first tens of seconds. Geophys. Res. Lett. 35, 6. https://doi.org/10.1029/2008GL033666.

Liu, J., Angelopoulos, V., Chu, X., Zhou, X.-Z., Yue, C., 2015. Substorm current wedge composition by wedgelets. Geophys. Res. Lett. 42 (6), 1669–1676. https://doi.org/10.1002/2015GL063289.

Liu, J., Lyons, L.R., Archer, W.E., Gallardo-Lacourt, B., Nishimura, Y., Zou, Y., et al., 2018. Flow shears at the poleward boundary of omega bands observed during conjunctions of swarm and THEMIS ASI. Geophys. Res. Lett. 45 (3), 1218–1227. https://doi.org/10.1002/2017GL076485.

Liu, J., Lyons, L.R., Wang, C.-P., Hairston, M.R., Zhang, Y., Zou, Y., 2020. Dawnside auroral polarization streams. J. Geophys. Res.: Space Phys. 125 (8), e2019JA027742 https://doi.org/10.1029/2019JA027742.

Lorentzen, D.A., Shumilov, N., Moen, J., 2004. Drifting airglow patches in relation to tail reconnection. Geophys. Res. Lett. 31 (2) https://doi.org/10.1029/2003GL017785.

Lui, A.T.Y., 1996. Current disruption in the Earth's magnetosphere: observations and models. J. Geophys. Res. Space Phys. 101, 13067–13088. https://doi.org/10.1029/96JA00079.

Lyons, L.R., 1996. Substorms: fundamental observational features, distinction from other disturbances, and external triggering. J. Geophys. Res. 101 (A6), 13011–13025. https://doi.org/10.1029/95JA01987.

Lyons, L.R., Nagai, T., Blanchard, G.T., Samson, J.C., Yamamoto, T., Mukai, T., et al., 1999. Association between Geotail plasma flows and auroral poleward boundary intensifications observed by CANOPUS photometers. J. Geophys. Res. 104 (A3), 4485–4500. https://doi.org/10.1029/1998JA900140.

Lyons, L.R., Nishimura, Y., Xing, X., Angelopoulos, V., Zou, S., Larson, D., et al., 2010a. Enhanced transport across entire length of plasma sheet boundary field lines leading to substorm onset. J. Geophys. Res. 115 https://doi.org/10.1029/2010JA015831.

Lyons, L.R., Nishimura, Y., Shi, Y., Zou, S., Kim, H.-J., Angelopoulos, V., et al., 2010b. Substorm triggering by new plasma intrusion: incoherent-scatter radar observations. J. Geophys. Res. 115 (A7) https://doi.org/10.1029/2009JA015168.

Lyons, L.R., Nishimura, Y., Kim, H.-J., Donovan, E., Angelopoulos, V., Sofko, G., et al., 2011. Possible connection of polar cap flows to pre- and post-substorm onset PBIs and streamers. J. Geophys. Res. 116, 14, 201110.1029/2011JA016850.

Lyons, L.R., Nishimura, Y., Xing, X., Runov, A., Angelopoulos, V., Donovan, E., Kikuchi, T., 2012. Coupling of dipolarization front flow bursts to substorm expansion phase phenomena within the magnetosphere and ionosphere. J. Geophys. Res. 117 (A2) https://doi.org/10.1029/2011JA017265.

Lyons, L.R., Nishimura, Y., Donovan, E., Angelopoulos, V., 2013a. Distinction between auroral substorm onset and traditional ground magnetic onset signatures. J. Geophys. Res.: Space Phys. 118 (7), 4080–4092. https://doi.org/10.1002/jgra.50384.

Lyons, L.R., Nishimura, Y., Gallardo-Lacourt, B., Zou, Y., Donovan, E., Mende, S., et al., 2013b. Westward traveling surges: sliding along boundary arcs and distinction from onset arc brightening. J. Geophys. Res.: Space Phys. 118 (12), 7643–7653. https://doi.org/10.1002/2013JA019334.

Lyons, L.R., Nishimura, Y., Gallardo-Lacourt, B., Nicolls, M.J., Chen, S., Hampton, D.L., et al., 2015. Azimuthal flow bursts in the inner plasma sheet and possible connection with SAPS and plasma sheet earthward flow bursts. J. Geophys. Res.: Space Phys. 120 (6) https://doi.org/10.1002/2015JA021023, 2015JA021023.

Lyons, Larry R., Wang, C.-P., Gkioulidou, M., Zou, S., 2009. Connections between plasma sheet transport, Region 2 currents, and entropy changes associated with convection, steady magnetospheric convection periods, and substorms. J. Geophys. Res.: Space Phys. 114 (A9), A00D01. https://doi.org/10.1029/2008JA013743.

Lyons, Larry R., Zou, Y., Nishimura, Y., Gallardo-Lacourt, B., Angelopulos, V., Donovan, E.F., 2018. Stormtime substorm onsets: occurrence and flow channel triggering. Earth Planets Space 70 (1), 81. https://doi.org/10.1186/s40623-018-0857-x.

Lyons, L.R., Liu, J., Nishimura, Y., Wang, C.-P., Reimer, A., Bristow, W.A., et al., 2020a. Radar observations of flows leading to longitudinal expansion of substorm onset over Alaska. J. Geophys. Res.

Lyons, L.R., Liu, J., Nishimura, Y., Reimer, A., Bristow, W.A., Hampton, D.L., et al., 2020b. Radar observations of flows leading to substorm onset over Alaska. J. Geophys. Res.

Machida, S., Miyashita, Y., Ieda, A., Nosé, M., Nagata, D., Liou, K., et al., 2009. Statistical visualization of the Earth's magnetotail based on Geotail data and the implied substorm model. Ann. Geophys. 27 (3), 1035–1046. https://doi.org/10.5194/angeo-27-1035-2009.

Makarevich, R.A., Kellerman, A.C., Devlin, J.C., Ye, H., Lyons, L.R., Nishimura, Y., 2011. SAPS intensification during substorm recovery: a multi-instrument case study. J. Geophys. Res. 116 (A11) https://doi.org/10.1029/2011JA016916.

McPherron, R.L., Russell, C.T., Aubry, M.P., 1973. 9. Phenomenological model for substorms. J. Geophys. Res. 78 (16), 3131–3149. https://doi.org/10.1029/JA078i016p03131.

Mende, S.B., Harris, S.E., Frey, H.U., Angelopoulos, V., Russell, C.T., Donovan, E., et al., 2008. The THEMIS array of ground-based observatories for the study of auroral substorms. Space Sci. Rev. 141 (1–4), 357–387. https://doi.org/10.1007/s11214-008-9380-x.

Moen, J., Gulbrandsen, N., Lorentzen, D.A., Carlson, H.C., 2007. On the MLT distribution of *F* region polar cap patches at night. Geophys. Res. Lett. 34 (14) https://doi.org/10.1029/2007GL029632.

Nagai, T., 1987. Field-aligned currents associated with substorms in the vicinity of synchronous orbit, 2. GOES 2 and GOES 3 observations. J. Geophys. Res. 92 (A3), 2432–2446.

Motoba, T., Hosokawa, K., Kadokura, A., Sato, N., 2012. Magnetic conjugacy of northern and southern auroral beads. Geophys. Res. Lett. 39 https://doi.org/10.1029/2012GL051599.

Nagai, Tsugunobu, 1982. Observed magnetic substorm signatures at synchronous altitude. J. Geophys. Res. 87 (A6), 4405–4417. https://doi.org/10.1029/JA087iA06p04405.

Nakamura, R., Baumjohann, W., Schödel, R., Brittnacher, M., Sergeev, V.A., Kubyshkina, M., et al., 2001. Earthward flow bursts, auroral streamers, and small expansions. J. Geophys. Res. 106 (A6), 10791–10802. https://doi.org/10.1029/2000JA000306.

Nicolls, M.J., Heinselman, C.J., 2007. Three-dimensional measurements of traveling ionospheric disturbances with the poker Flat incoherent scatter radar. Geophys. Res. Lett. 34 (21) https://doi.org/10.1029/2007GL031506.

Nishida, A., Kokubun, S., 1971. New polar magnetic disturbances: S q p , SP , DPC , and DP 2. Rev. Geophys. 9 (2), 417. https://doi.org/10.1029/RG009i002p00417.

Nishimura, Y., Lyons, L., Zou, S., Angelopoulos, V., Mende, S., 2010a. Substorm triggering by new plasma intrusion: THEMIS all-sky imager observations. J. Geophys. Res. 115 (A7) https://doi.org/10.1029/2009JA015166.

Nishimura, Y., Lyons, L.R., Zou, S., Angelopoulos, V., Mende, S.B., 2010b. Reply to comment by Harald U. Frey on "Substorm triggering by new plasma intrusion: THEMIS all-sky imager observations. J. Geophys. Res. 115 (A12) https://doi.org/10.1029/2010JA016182.

Nishimura, Y., Lyons, L.R., Zou, S., Angelopoulos, V., Mende, S.B., 2011a. Categorization of the time sequence of events leading to substorm onset based on THEMIS all-sky imager observations. In: Liu, W., Fujimoto, M. (Eds.), The Dynamic Magnetosphere. Springer Netherlands, Dordrecht, pp. 133–142. http://www.springerlink.com/content/x170k84772368516/.

Nishimura, Y., Lyons, L.R., Angelopoulos, V., Kikuchi, T., Zou, S., Mende, S.B., 2011b. Relations between multiple auroral streamers, pre-onset thin arc formation, and substorm auroral onset. J. Geophys. Res.: Space Phys. 116 (A9), A09214. https://doi.org/10.1029/2011JA016768.

Nishimura, T., Lyons, L.R., Kikuchi, T., Angelopoulos, V., Donovan, E.F., Mende, S.B., et al., 2012a. Formation of substorm Pi 2: a coherent response to auroral streamers and currents. J. Geophys. Res. https://doi.org/10.1029/2012JA017889.

Nishimura, Y., Lyons, L.R., Kikuchi, T., Angelopoulos, V., Donovan, E.F., Mende, S.B., Lühr, H., 2012b. Relation of substorm pre-onset arc to large-scale field-aligned current distribution. Geophys. Res. Lett. 39 (22) https://doi.org/10.1029/2012GL053761 n/a–n/a.

Nishimura, Y., Lyons, L.R., Shiokawa, K., Angelopoulos, V., Donovan, E.F., Mende, S.B., 2013a. Substorm onset and expansion phase intensification precursors seen in polar cap patches and arcs. J. Geophys. Res.: Space Phys. 118 (5), 2034–2042. https://doi.org/10.1002/jgra.50279.

Nishimura, Y., Lyons, L.R., Xing, X., Angelopoulos, V., Donovan, E.F., Mende, S.B., et al., 2013b. Tail reconnection region versus auroral activity inferred from conjugate ARTEMIS plasma sheet flow and auroral observations. J. Geophys. Res.: Space Phys. 118 (9), 5758–5766. https://doi.org/10.1002/jgra.50549.

Nishimura, Y., Lyons, L.R., Nicolls, M.J., Hampton, D.L., Michell, R.G., Samara, M., et al., 2014. Coordinated ionospheric observations indicating coupling between preonset

flow bursts and waves that lead to substorm onset. J. Geophys. Res.: Space Phys. 119 (5), 3333–3344. https://doi.org/10.1002/2014JA019773.
Nishimura, Y., Yang, J., Pritchett, P.L., Coroniti, F.V., Donovan, E.F., Lyons, L.R., et al., 2016. Statistical properties of substorm auroral onset beads/rays. J. Geophys. Res.: Space Phys. 121 (9), 8661–8676. https://doi.org/10.1002/2016JA022801.
Ogasawara, K., Kasaba, Y., Nishimura, Y., Hori, T., Takada, T., Miyashita, Y., et al., 2011. Azimuthal auroral expansion associated with fast flows in the near-Earth plasma sheet: coordinated observations of the THEMIS all-sky imagers and multiple spacecraft. J. Geophys. Res.: Space Phys. 116 (A6) https://doi.org/10.1029/2010JA016032.
Ohtani, S., 1998. Earthward expansion of tail current disruption: dual-satellite study. J. Geophys. Res. 103, 6815–6825.
Palin, L., Jacquey, C., Opgenoorth, H., Connors, M., Sergeev, V., Sauvaud, J.-A., et al., 2015. Three-dimensional current systems and ionospheric effects associated with small dipolarization fronts. J. Geophys. Res.: Space Phys. 120 (5), 3739–3757. https://doi.org/10.1002/2015JA021040.
Panov, E.V., Nakamura, R., Baumjohann, W., Angelopoulos, V., Petrukovich, A.A., Retinò, A., et al., 2010. Multiple overshoot and rebound of a bursty bulk flow. Geophys. Res. Lett. 37 (8) https://doi.org/10.1029/2009GL041971 n/a–n/a.
Panov, E.V., Sergeev, V.A., Pritchett, P.L., Coroniti, F.V., Nakamura, R., Baumjohann, W., et al., 2012. Observations of kinetic ballooning/interchange instability signatures in the magnetotail. Geophys. Res. Lett. 39 (8) https://doi.org/10.1029/2012GL051668.
Park, M.Y., Lee, D.-Y., Ohtani, S., Kim, K.C., 2010. Statistical characteristics and significance of low-frequency instability associated with magnetic dipolarizations in the near-Earth plasma sheet. J. Geophys. Res. 115 (A11), A11203. https://doi.org/10.1029/2010JA015566.
Pitkänen, T., Aikio, A.T., Amm, O., Kauristie, K., Nilsson, H., Kaila, K.U., 2011. EISCAT-Cluster observations of quiet-time near-Earth magnetotail fast flows and their signatures in the ionosphere. Ann. Geophys. 29 (2), 299–319. https://doi.org/10.5194/angeo-29-299-2011.
Pitkänen, T., Aikio, A.T., Juusola, L., 2013. Observations of polar cap flow channel and plasma sheet flow bursts during substorm expansion. J. Geophys. Res.: Space Phys. 118 (2), 774–784. https://doi.org/10.1002/jgra.50119.
Pontius, D.H., Wolf, R.A., 1990. Transient flux tubes in the terrestrial magnetosphere. Geophys. Res. Lett. 17 (1), 49–52. https://doi.org/10.1029/GL017i001p00049.
Pritchett, P.L., Coroniti, F.V., Nishimura, Y., 2014. The kinetic ballooning/interchange instability as a source of dipolarization fronts and auroral streamers. J. Geophys. Res.: Space Phys. 119 (6), 4723–4739. https://doi.org/10.1002/2014JA019890.
Pytte, T., Mcpherron, R.L., Kokubun, S., 1976. The ground signatures of the expansion phase during multiple onset substorms. Planet. Space Sci. 24 (12) https://doi.org/10.1016/0032-0633(76)90149-5, 1115-IN4.
Rae, I.J., Watt, C.E.J., Mann, I.R., Murphy, K.R., Samson, J.C., Kabin, K., Angelopoulos, V., 2010. Optical characterization of the growth and spatial structure of a substorm onset arc. J. Geophys. Res. 115 (A10), A10222. https://doi.org/10.1029/2010JA015376.
Rae, I. Jonathan, Mann, I.R., Angelopoulos, V., Murphy, K.R., Milling, D.K., Kale, A., et al., 2009. Near-Earth initiation of a terrestrial substorm. J. Geophys. Res. 114 (A7), A07220. https://doi.org/10.1029/2008JA013771.
Rostoker, G., 1968. Macrostructure of geomagnetic bays. J. Geophys. Res. 73 (13), 4217–4229. https://doi.org/10.1029/JA073i013p04217.
Rostoker, G., Akasofu, S.-I., Foster, J., Greenwald, R.A., Kamide, Y., Kawasaki, K., Lui, A. T.Y., McPherron, R.L., Russell, C.T., 1980. Magnetospheric substorms—definition and signatures. J. Geophys. Res. 85, 1663–1668. https://doi.org/10.1029/JA085iA04p01663.
Roux, A., Perraut, S., Robert, P., Morane, A., Pedersen, A., Korth, A., et al., 1991. Plasma sheet instability related to the westward traveling surge. J. Geophys. Res. 96 (A10) https://doi.org/10.1029/91JA01106, 17697–17,714.
Sakaguchi, K., Shiokawa, K., Ieda, A., Nomura, R., Nakajima, A., Greffen, M., et al., 2009. Fine structures and dynamics in auroral initial brightening at substorm onsets. Ann. Geophys. 27 (2), 623–630. https://doi.org/10.5194/angeo-27-623-2009.
Sakurai, T., Saito, T., 1976. Magnetic pulsation Pi2 and substorm onset. Planet. Space Sci. 24 (6), 573–575. https://doi.org/10.1016/0032-0633(76)90135-5.
Samson, J.C., Lyons, L.R., Newell, P.T., Creutzberg, F., Xu, B., 1992. Proton aurora and substorm intensifications. Geophys. Res. Lett. 19 (21), 2167. https://doi.org/10.1029/92GL02184.
Sergeev, V., Nishimura, Y., Kubyshkina, M., Angelopoulos, V., Nakamura, R., Singer, H., 2012. Magnetospheric location of the equatorward prebreakup arc. J. Geophys. Res. 117 (A1) https://doi.org/10.1029/2011JA017154.
Sergeev, V.A., 1974. On the longitudinal localization of the substorm active region and its changes during the substorm. Planet. Space Sci. 22 (9), 1341–1343. https://doi.org/10.1016/0032-0633(74)90055-5.
Sergeev, V.A., Angelopoulos, V., Gosling, J.T., Cattell, C.A., Russell, C.T., 1996. Detection of localized, plasma-depleted flux tubes or bubbles in the midtail plasma sheet. J. Geophys. Res.: Space Phys. 101 (A5), 10817–10826. https://doi.org/10.1029/96JA00460.
Sergeev, V.A., Liou, K., Meng, C.-I., Newell, P.T., Brittnacher, M., Parks, G., Reeves, G.D., 1999. Development of auroral streamers in association with localized impulsive injections to the inner magnetotail. Geophys. Res. Lett. 26 (3), 417–420, 199910.1029/1998GL900311.
Sergeev, V.A., Sauvaud, J.-A., Popescu, D., Kovrazhkin, R.A., Liou, K., Newell, P.T., et al., 2000. Multiple-spacecraft observation of a narrow transient plasma jet in the Earth's plasma sheet. Geophys. Res. Lett. 27 (6), 851–854, 200010.1029/1999GL010729.
Shi, Y., Zesta, E., Lyons, L.R., Yang, J., Boudouridis, A., Ge, Y.S., et al., 2012. Two-dimensional ionospheric flow pattern associated with auroral streamers. J. Geophys. Res. 117 (A2) https://doi.org/10.1029/2011JA017110.
Shiokawa, K., Ieda, A., Nakajima, A., Sakaguchi, K., Nomura, R., Aslaksen, T., et al., 2009. Longitudinal development of a substorm brightening arc. Ann. Geophys. 27 (5), 1935–1940. https://doi.org/10.5194/angeo-27-1935-2009.
Shiokawa, K., Miyashita, Y., Shinohara, I., Matsuoka, A., 2005. Decrease in Bz prior to the dipolarization in the near-Earth plasma sheet. J. Geophys. Res. Space Phys. 110 https://doi.org/10.1029/2005JA011144.
Silsbee, H.C., Vestine, E.H., 1942. Geomagnetic bays, their frequency and current-systems. Terr. Magnetism Atmos. Electr. 47 (3), 195–208. https://doi.org/10.1029/TE047i003p00195.
Takahashi, K., Zanetti, L.J., Lopez, R.E., McEntire, R.W., Potemra, T.A., Yumoto, K., 1987. Disruption of the magnetotail current sheet observed by AMPTE/CCE. Geophys. Res. Lett. 14, 1019–1022.
Uritsky, V.M., Liang, J., Donovan, E., Spanswick, E., Knudsen, D., Liu, W., et al., 2009. Longitudinally propagating arc wave in the pre-onset optical aurora. Geophys. Res. Lett. 36 (21) https://doi.org/10.1029/2009GL040777.
Wang, C.-P., Gkioulidou, M., Lyons, L.R., Wolf, R.A., 2018. Spatial distribution of plasma sheet entropy reduction caused by a plasma bubble: Rice convection model simulations. J. Geophys. Res.: Space Phys. 123 (5), 3380–3397. https://doi.org/10.1029/2018JA025347.
Wolf, R.A., Chen, C.X., Toffoletto, F.R., 2012. Thin filament simulations for Earth's plasma sheet: interchange oscillations. J. Geophys. Res.: Space Phys. 117 (A2) https://doi.org/10.1029/2011JA016971 n/a–n/a.
Xing, X., Wolf, R.A., 2007. Criterion for interchange instability in a plasma connected to a conducting ionosphere. J. Geophys. Res.: Space Phys. 112 (A12), A12209. https://doi.org/10.1029/2007JA012535.
Xing, X., Lyons, L., Nishimura, Y., Angelopoulos, V., Larson, D., Carlson, C., et al., 2010. Substorm onset by new plasma intrusion: THEMIS spacecraft observations. J. Geophys. Res.-Space Phys. 115 https://doi.org/10.1029/2010JA015528.
Yang, J., Toffoletto, F.R., Wolf, R.A., Sazykin, S., 2011. RCM-E simulation of ion acceleration during an idealized plasma sheet bubble injection. J. Geophys. Res. 116 https://doi.org/10.1029/2010JA016346.
Yang, Jian, Toffoletto, F.R., Wolf, R.A., 2014. RCM-E simulation of a thin arc preceded by a north-south-aligned auroral streamer. Geophys. Res. Lett. 41 (8), 2695–2701. https://doi.org/10.1002/2014GL059840.
Zesta, E., Lyons, L., Donovan, E., 2000. The auroral signature of Earthward flow bursts observed in the Magnetotail. Geophys. Res. Lett. 27 (20), 3241–3244.
Zou, S., Lyons, L.R., Nicolls, M.J., Heinselman, C.J., Mende, S.B., 2009. Nightside ionospheric electrodynamics associated with substorms: PFISR and THEMIS ASI observations. J. Geophys. Res.: Space Phys. 114 (A12) https://doi.org/10.1029/2009JA014259 n/a–n/a.
Zou, Y., Nishimura, Y., Lyons, L.R., Donovan, E.F., Ruohoniemi, J.M., Nishitani, N., McWilliams, K.A., 2014. Statistical relationships between enhanced polar cap flows and PBIs. J. Geophys. Res.: Space Phys. 119 (1) https://doi.org/10.1002/2013JA019269, 2013JA019269.